Master thesis

Modeling and State Estimation Algorithm Development for Lithium-ion Battery Cells

Master thesis in Electric Power Engineering

Saraswathi Vinod

CHALMERS
UNIVERSITY OF TECHNOLOGY

Institution of Electrical Engineering
Department of Electric Power Engineering
Chalmers University of Technology
Gothenburg, Sweden 2023

Master Thesis in Electric Power Engineering

Saraswathi Vinod

Supervisor: Yizhou Zhang
Examiner: Changfu Zou

Master Thesis
Department of Electrical Engineering
Division of Electric Power Engineering
Chalmers University of Technology
SE-412 96 Gothenburg
Sweden
Phone: +46 31 772 1000

Abstract

In recent years there has been a lot of research and money invested in the development of electric vehicles. Since it is a newer technology there is much to be understood and improved. The lithium-ion battery is an important and expensive part of the electric driveline and many other electric systems. Optimizing test methods and prediction of its state of charge and lifetime is an area of interest. This will help reduce the price and weight and improve the utilization of the battery pack. This thesis is focused on the testing, modeling, and state and parameter estimation of a commercially available lithium-ion cell. 8 lithium-ion cells were tested at 25°C in different SOC windows with WLTP cycles to emulate real-life driving situations. Amongst the SOC windows tested the (50-100)% window showed the least capacity degradation. The cell was modeled using parameters found from the reference performance tests (RPT) and the 2 RC model was found to be slightly more accurate than the 1 RC model for WLTP cycling. However, due to lower complexity, the 1 RC model was chosen to perform state estimation. The extended Kalman filter method estimated the SOC to an accuracy of 1.3%. A joint Kalman filter to estimate the model parameters and capacity along with SOC was also implemented.

Acknowledgements

I would like to thank Yizhou Zhang for his support and guidance as our project supervisor during this thesis.

I would also like to thank my examiner, Professor Changfu Zou for his feedback which helped improve the direction and quality of the work done in this thesis.

I am very grateful to Thompson Akinyokun of KTH University who was my teammate in this thesis work. I am thankful for his ideas, support, and hard work while overcoming challenges in this thesis.

I am also thankful to Niharika and Vaghul for being the opposition during my thesis presentation and asking interesting questions.

I am grateful to my family and friends for their support and encouragement.

Abbreviations

Abbreviation	Meaning
BOL	Beginning of Life
EOL	End of Life
SOC	State of Charge
SOH	State of Health
SOP	State of Power
SOE	State of Energy
RC	Resistor Capacitor
EFC	Equivalent Full Cycles
KF	Kalman Filter
EKF	Extended Kalman Filter
OCV	Open Circuit Voltage
ACT	Advanced Cell Tester
RPT	Reference Performance Tests
WLTP	Worldwide harmonized Light Vehicle Test Procedure
CCCV	Constant Current Constant Voltage
ECM	Equivalent Circuit Model
Li-ion	Lithium-Ion
BMS	Battery Management System
NMC	Nickel Manganese Cobalt oxide
RMS	Root Mean Square
RMSE	Root Mean Square Error
HPPC	Hybrid Pulse Power Characterization Test
ACT	Advanced Cell Tester
BEV	Battery Electric Vehicle
JEKF	Joint Extended Kalman Filter
SEI	Solid Electrolyte Interface
DOD	Depth of Discharge

Symbols

Symbol	Meaning
R_0	Resistor modeling instantaneous change in 1 RC and 2 RC models
R_1	Resistor in the 1st RC branch in the 1 RC and 2 RC models
R_2	Resistor in the 2nd RC branch in the 2 RC model
C_1	Capacitor in the 1st RC branch in the 1 RC and 2 RC models
C_2	Capacitor in the 2nd RC branch in the 2 RC models
I	Current from the cell (charge current positive)
I_{R1}	Current through R_1
I_{R2}	Current through R_2
η	Coulombic efficiency
L	Kalman gain
Q	Rated capacity of a cell at BOL
z	SOC (in per unit) expressed between 0 and 1
T_s	Sample Time
V_t	Terminal Voltage
v	Signal modelling sensor noise
w	Signal modelling process noise
Σ_V	Covariance matrix of sensor noise
Σ_W	Covariance matrix of process noise
Σ_X	Covariance matrix of measurement update error
$\hat{x}$	a ˆ symbol on a variable indicates an estimate of the variable
A, B, C, D	Matrices in the state space representation
x	State vector
u	Input vector
y	Output vector

Contents

Chapter 1

Introduction

1.1 Background

Electrification of transport is gaining momentum across Europe and the world. Batteries play a significant role in making the transition to electric vehicles successful. Due to features such as high energy, high power, and long lifetime, lithium-ion (Li-ion) batteries are considered a favorable option for use in electric vehicles. In this thesis, the commercially available cylindrical NMC 811 cells, which is a type of Li-ion cell, were studied. These are cells with a cathode composition of 80% Nickel, 10% Manganese and 10% Cobalt [1].

Li-ion batteries exhibit non-linear behavior and varying characteristics with age, usage, and other factors such as temperature. This makes it challenging to build models that can accurately predict the behavior of the cell under all conditions. An accurate battery model is imperative for the Battery Management System (BMS) to make sufficient estimation of the battery states and to be able to utilize the battery efficiently. Static battery models which are characterized by a few laboratory tests can lead to errors during actual usage. Since battery model parameters like the internal resistance and cell capacity can vary with battery age and operating conditions, the need for an adaptive model arises. Thus, a model that will update model parameters taking the variations into account is needed. The battery usage has to be controlled in real-time, this requires that the model also needs to function online and in real-time. Additionally, a balance must be struck between model accuracy and model complexity so that while staying mostly accurate, the model can be embedded in microprocessors and be computed in real-time.

Models commonly used to characterize batteries can be broadly classified into Equivalent Circuit models, Physics-based electrochemical models, and Data-driven models [2]. Physics-based electrochemical models can achieve high accuracy but contain a large number of unknown parameters which can lead to high complexity and overfitting problems [3]. Several Equivalent Circuit Models have been proposed for Li-ion batteries [3] such as the first-order RC circuit, Randel's model, higher-order RC circuits, RC models with hysteresis included, etc. These have lumped parameters which

are much fewer in number compared to the physics-based model, making the models less complex. However, the models can still reach adequate levels of accuracy. Different methods have been studied to characterize the parameters of these equivalent circuit models. The models that are linear in their parameters can use least squares methods such as in [4]. This method can help compute the parameters online. For models that are non-linear in their parameters, the Kalman filter can be used to estimate the parameter when its dynamic model is known [5].

Given a battery, there are not many quantities that can be directly, or physically measured from it. It is usually the terminal voltage, current, and temperature that can be obtained as physical signals. However, there are other internal states of the battery such as its State of Charge (SOC), State of Health (SOH), and State of Energy (SOE) that are needed to make decisions on how to best utilize the battery. For instance, the SOE will give an estimate of the remaining energy and thus help determine the remaining range of the vehicle. These states of the battery must be estimated from the available data. Improvements in the accuracy of these estimates have the potential to improve battery life, performance, and density. A more accurate estimation of SOC can help improve the longevity of the battery by preventing over-charging or over-discharging. The performance improves as the same battery can be utilized more aggressively when the estimation error is minimized. This is because the conservative safety margins required to account for the estimation error are also reduced. This means that the batteries can be more fully utilized which will imply smaller batteries for the same purpose and increased useful energy density of the battery [6].

Different state estimation algorithms have been researched to estimate the internal states of a battery [7]. Methods such as Coulomb counting, and OCV mapping are some conventional ways of SOC determination. These methods have however proved not to be very useful for real-time state estimation. Usage of an Extended Kalman Filter (EKF) technique to implement the SOC estimation has been suggested in [8] and is a method that can be used for more dynamic state estimations.

The importance of good-quality data on the cell cannot be overlooked while building a cell model. Testing the cell in different conditions and under different loads can provide a lot of information on the cell. This helps to tune the model of the cell. The temperatures surrounding the cells can be varied, and so can the humidity and the type of drive cycle. In between these tests, it becomes necessary to also run reference tests so that the cell parameter changes as the cell ages can be tracked. Thus, testing is also an equally important focus of this thesis, to collect data on the cell.

1.2 Aim

The thesis aimed to build a battery model based on testing data from commercially available NMC811 cylindrical cells. This was to be followed by the implementation of intelligent battery state estimation algorithms in a simulation environment.

1.3 Scope

The full scope of the project is listed below as

- Performing battery cell testing to collect data for the thesis and characterize the cell during its lifetime.
- Calibrating equivalent circuit models based on the collected data. Attempting to make these models online implementable and adaptive.
- Programming cell-level estimation algorithms to estimate states such as SOC and SOH.

The effects of regenerative braking on the cell lifetime will not be accounted for while performing the tests on the battery cells. In addition, the thermal impact on cell degradation and aging will also not be accounted for.

Chapter 2

Theoretical Background

This Chapter presents the basic background theory of this thesis. The working principle of lithium-ion cells is presented. The overall function of the Battery Management System (BMS) is explained highlighting its basic functions. The term State of Charge (SOC) is explained. The aging of cells is covered and the term State of Health (SOH) is introduced. Different methods for modeling batteries are introduced and the electrical equivalent model is represented as a State Space Model. Finally, the theory of Kalman filters is introduced explaining the the Linear and Extended Kalman filters.

2.1 Lithium-Ion Battery Cells

In lithium-ion cells, lithium ions move from the anode (negative electrode) to the cathode (positive electrode) through an electrolyte during the discharge of the cell. When the cell is charged this reaction is reversed, making lithium-ion cells rechargeable cells. There are different chemistries of Li-ion cells usually classified based on what kind of cathode is used. Some of the common cathode compositions are Lithium Nickel Manganese Cobalt Oxides (NMC), Lithium Iron Phosphate (LFP), Lithium Nickel Cobalt Aluminium Oxide (NCA), Lithium Cobalt Oxide (LCO), etc. Conventionally, the anodes are made of graphite and other carbon materials. In recent times, additions of Silicon are also made to the anode as this increases the capacity of the cells. However, it can lead to some other problems such as the anode being brittle due to the expansion of the Silicon-Lithium combination. The electrolyte in the lithium-ion cell is usually a lithium salt (eg. $LiPF_6$) in an organic solvent. Lithium Nickel Manganese Cobalt Oxide (NMC) battery cells are common within the automotive industry. This is because NMC cells possess a comparatively high energy density but it comes at the cost of utilizing Nickel and Cobalt which are expensive minerals and raise sustainability and ethics issues due to the mining of these minerals.

2.2 Battery Management System

The BMS is a safety critical component of the energy storage system whose purpose is to keep the battery operating in safe operating conditions and communicate the state

of the battery to surrounding subsystems. In an electric powertrain, for instance, the battery voltage will influence the switching losses of the inverter, and when the electric machine enters the field weakening it will influence the phase currents and the losses of the electric machine. The BMS will also monitor the temperatures, currents, and voltages of the cells within the battery pack to ensure that all of these parameters stay within the rated operational regions of the cells. Should any of the ingoing signals into the BMS indicate that one or more parameters are not within the specified operating region, either derate functions on the powertrain will be set to reduce the stress on the battery or the entire vehicle will enter a safe state and the battery will be disconnected from the rest of the vehicle. Apart from monitoring the battery to ensure safety, the battery management system also estimates the states of the battery, such as the state of charge (Section 2.3), state of power, etc. The BMS also performs fault diagnostics which informs the user of failures that have occurred.

2.3 State of Charge (SOC)

State of charge is the amount of remaining charge in a cell relative to its rated capacity. The rated capacity of the cell is the amount of charge that can be taken out from the cell and is usually expressed in Ah. A battery cell with a rated capacity of 30 Ah has enough charge when fully charged to deliver 30 A current for an hour or to give 3 A current for 10 hours. The State of Charge of the cell can be expressed in a percentage of or ratio of the rated capacity. The SOC is measured between 0 % - 100 % or 0-1. The SOC is 0 % or 0 when the cell is fully discharged and 100% or 1 when the cell is fully charged. The Depth of Discharge (DoD) is a quantity directly resulting from the SOC. It is calculated as 1-SOC or 100 %- SOC(in %). It is a measure of how discharged the cell is from its fully charged state.

The state of charge unlike the terminal voltage or current of the cell is not directly measurable but a hidden quantity that is important. In different applications, knowledge of the state of charge is very useful. For instance, while driving an electric car it is crucial to know the state of charge to be able to predict the remaining range of the car. Accurately determining the state of charge can prevent accidental over-discharging or overcharging of the cell and allow for more efficient use of the battery pack.

2.3.1 SOC Calculation

The SOC at a time point t, in continuous time, is given by,

$$SOC(t) = SOC(t_0) + \frac{\eta \int_{t_0}^{t} I(p)\ dp}{Q} * 100 \tag{2.1}$$

where SOC(t) is the SOC at time t in %, SOC(t_0) is the initial SOC or the SOC at time t_0, I(p) is the current in A and is positive for charging, η is the coulombic efficiency and Q is the rated capacity of the cell in Ah. The capacity Q of the cell is considered constant in Equation 2.1. However, in real life, the capacity of the cell reduces as the cell ages. However, the time scale for significant changes in capacity is much larger than

the time scale for SOC changes, hence the capacity can be assumed to stay constant at this stage. For simulations, it is useful to have the discrete-time equation of the SOC and it is,

$$SOC[k] = SOC[k-1] + \frac{\eta T_s I[k-1]}{Q * 3600} * 100 \tag{2.2}$$

where SOC[k] is the SOC in %, T_s time after SOC[k-1], T_s is the sample time in seconds and I[k-1] is the current (positive for charging) in A during this sampling period. In this thesis report the variable z[k] is used to represent the SOC represented between 0 and 1.

2.3.2 Coulomb Counting

Coulomb counting is an easy and common method to determine the SOC of the battery cell. It uses the basic equation defined in Equation 2.1. The current drawn from the cell is integrated over time to find the charge lost which gives the depletion of the state of charge. However, this method is dependent on how accurate the current measurement is and any errors or bias in the measurement can lead to an accumulating error that will grow over time. As can be seen from Equation 2.1, it is crucial to know the initial state of charge of the cell to use this method. To overcome this drawback other algorithms are proposed and one of them involves the usage of an Extended Kalman Filter.

2.4 Aging and State of Health (SOH)

As a battery cell is used or even when it is just sitting idle, it ages. When the cell ages due to operation it is called cyclical aging and when it ages during storage or sitting idle it is called calendric aging. Most cells age due to a combination of the two since they are not always in operation. As a cell ages, it undergoes several changes internally which in general decrease its performance. This makes it crucial to understand the aging of batteries since a brand-new cell will behave quite differently from a cell of the same model that has been used for a year.

Usually, the internal resistance of the cell goes up with age. This makes the power that can be drawn from the cell to decrease. The capacity of the cell also goes down with age. The cell is said to have reached its end of life (EOL) for automotive applications usually when its capacity has reached around 80 % of what it was during its beginning of life. This reducing capacity is an indicator of the State of Health (SOH) of the cell. When the cell is first produced, it has a State of Health of 100 %. As the cell ages its State of Health goes down. A cell whose capacity has gone down to 95 % of its initial capacity is said to have an SOH of 95 %. After the end-of-life batteries can often be used for less critical applications such as stationary energy storage systems. These batteries are said to be in second-life applications.

2.5 Battery Cell Models

A battery cell has non-linear characteristics and capturing all its behavior cannot be accomplished with simple models. With models of battery cells, there is often a balance to be struck between accuracy and complexity. Very complex models can be built but they can be computationally heavy meaning that a significant amount of computational power is needed to perform the calculations. In applications such as automotive applications, having such a computationally heavy model is not useful due to the restricted computational power on the BMS. Several types of models have been proposed for battery systems, some of which are presented here.

2.5.1 Physics-based Model

The Physics-based models take into consideration the fundamental electrochemical events that occur in a Li-ion cell during charge and discharge. The physics-based model uses mathematical equations to model these electrochemical events and uses that to predict a cell's performance and lifetime. Some examples of quantities that can be modeled are Li-ion concentration, diffusion potential in the cell, etc. In addition, the models can account for thermal effects such as heat generation, heat transfer, and thermal expansion of the cells.

Methods such as Finite Element Method are used to build and solve such models [9]. These models can have quite a high accuracy as compared to the other stated modeling techniques but come with the cost of high computational load. Some models developed are the Doyle–Fuller–Newman (DFN) battery model [10] and the Single Particle Model (SPM) [11].

2.5.2 Electrical Equivalent Model

Modeling a battery cell using the electrical equivalent models means modeling the characteristics and behavior of the cell using circuit elements. When current passes through the cell, the terminal voltage of the cell changes from the OCV. Any such change is considered due to a polarization voltage and resistive voltage drop. Figure 2.1 shows the terminal voltage of a cell when a discharge pulse is applied to it. As seen in Figure 2.1, there is a change in voltage that happens instantaneously and another that happens gradually. Also when the cell is allowed to rest the voltage returns to OCV only gradually. This relationship between the current and voltage of a cell is quite similar to that in RC circuits. While a cell can be modeled quite simply as a voltage source in series with a resistor, this does not fully capture the behavior, especially the dynamic variations in the cell. It only captures the instantaneous behavior. Additions of RC branches lead to capturing the slow changes, with each extra RC making the voltage change even smoother and closer to the real changes seen in a cell. However, more RC branches add to the complexity and computational time of the model. Figure 2.2 shows the equivalent circuit model of a cell model using a 1 RC circuit. R_0 captures the instantaneous voltage change and the R_1, C_1 combination captures the slow changes in terminal voltage. The OCV is modeled to be dependent on SOC and the temperature of the cell.

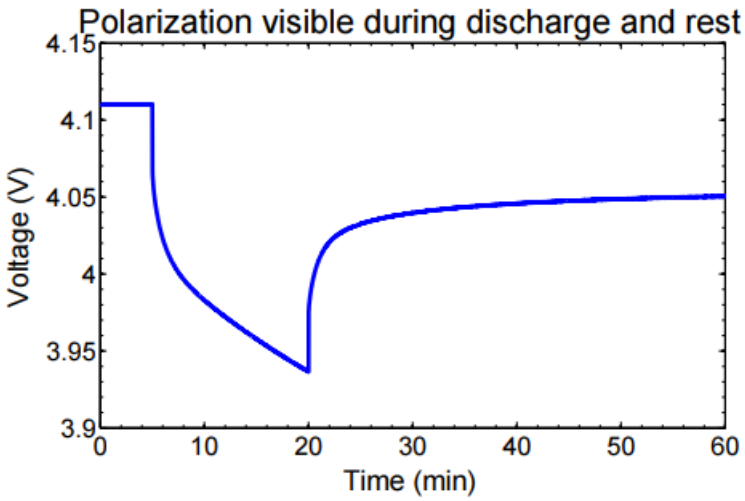

Figure 2.1: Polarization in the terminal voltage [12]

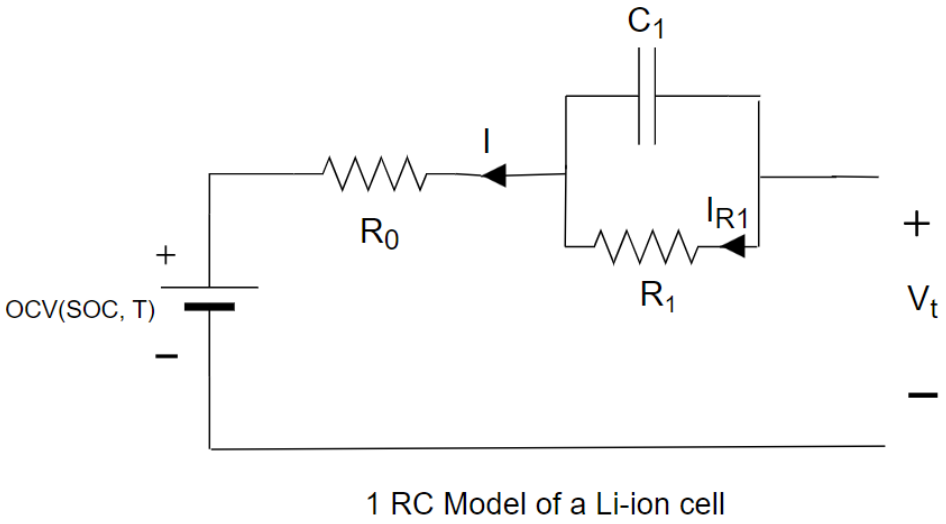

Figure 2.2: Equivalent circuit model with 1 RC branch

The cell terminal voltage $V_t(t)$ in V can be represented as

$$V_t(t) = OCV(SOC, T)(t) + I(t)R_0 + I_{R1}(t)R_1 \tag{2.3}$$

where, quantities are defined at time t, OCV(SOC,T) is the temperature(T)- and SOC-dependent OCV, I is the cell current, I_{R1} is the modeled current through the resistor of the 1RC branch. R_0, R_1, and C_1 are the resistances (in Ω) and capacitance (in F) defined for this model. They are considered time invariant in Equation 2.3, however, they can change with the age and SOC of the cell. But they vary quite slowly compared to the other quantities and hence are assumed constant in Equation 2.3.

The relationship between the current I_{R1} and I can be found by using basic circuit theory to be

$$\dot{I}_{R1}(t) = -\frac{I_{R1}(t)}{R_1 C_1} + \frac{I(t)}{R_1 C_1} \tag{2.4}$$

where $\dot{I}_{R1}(t)$ is the time derivative of the current I_{R1} and the other variables are the same as described for Equation 2.3. In discrete time Equation 2.4 can be written as

$$I_{R1}[k] = e^{\frac{-T_s}{R_1 C_1}} I_{R1}[k-1] + (1 - e^{\frac{-T_s}{R_1 C_1}}) I[k-1] \tag{2.5}$$

where what the variables stand for remains the same but they are defined at samples of k or k+1 instead of in continuous time. Figure 2.3 shows the 2RC model of a cell. It has an additional RC branch to capture the dynamic change even smoother than the 1 RC circuit.

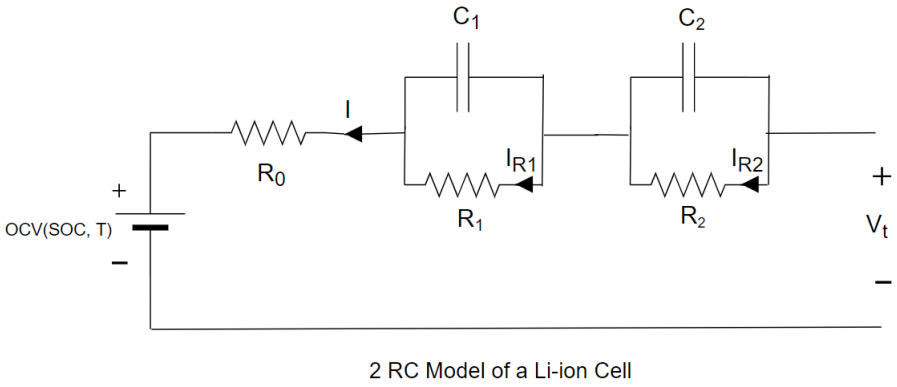

Figure 2.3: Equivalent circuit model with 2 RC branches

In a 2RC model as shown in Figure 2.3, the cell terminal voltage $V_t(t)$ in V can be represented as

$$V_t(t) = OCV(SOC, T)(t) + I(t)R_0 + I_{R1}(t)R_1 + I_{R2}(t)R_2 \tag{2.6}$$

where, I_{R2} is the current through the resistor of the 2nd RC branch. R_0, R_1, R_2, C_1, and C_2 are the resistances and capacitances defined for this model. They are considered time-invariant in Equation 2.6, however, they can change with the age and SOC of the cell. But they vary quite slowly compared to the other quantities and hence are assumed constant in Equation 2.6.

The relationship between the current I_{R1} and I is the same as in Equation 2.3 and I_{R2} and I is similar and

$$\dot{I}_{R2}(t) = -\frac{I_{R2}(t)}{R_2 C_2} + \frac{I(t)}{R_2 C_2} \tag{2.7}$$

where the variables are the same as described for Equation 2.6. In discrete time Equation 2.7 can be written as

$$I_{R2}[k] = e^{\frac{-T_s}{R_2 C_2}} I_{R2}[k-1] + (1 - e^{\frac{-T_s}{R_2 C_2}}) I[k-1] \tag{2.8}$$

where what the variables stand for remains the same but they are defined at samples of k or k+1 instead of in continuous time.

2.5.3 Data-based Model

A data-based battery cell model utilizes neural networks and machine learning to predict the behavior of the battery. These kinds of methods have proven to be effective for modeling the lifetime degradation of the cells and predicting battery parameters. These models use cell data either recorded by the monitoring system in the battery pack or utilize experimentally obtained data. [13].

2.6 State Space Representation

A system can be modeled mathematically through state space representation. Here the relations are specified in terms of inputs, states, and outputs. States define the state of the system completely at any given time. The state space model consists of 2 sets of equations, one is the group of equations for the states, and the other is the group of equations for the outputs. At any given time a state is dependent on its history and the input at the current time. At any given time the output is dependant on both the states and the inputs. Usually, it is the inputs and outputs that are accessible or measurable from the system. The states are more hidden quantities.

The simplest form of state space representation for a linear, time-invariant system in continuous time is

$$\begin{aligned} \dot{x}(t) &= Ax(t) + Bu(t) && (2.9) \\ y(t) &= Cx(t) + Du(t) && (2.10) \end{aligned}$$

where, x(t) is the state vector at time t and of length n, u(t) is the input vector at time t, and of length m, y(t) is the output vector at time t and of length q. A, B, C, and D are matrices of size n x n, n x m, q x n and q x m respectively. A is the state (or system) matrix, B is the input matrix, C is the output matrix and D is the feedforward matrix. The state space representation can also be drawn for a linear, time-invariant system in discrete-time as,

$$\begin{aligned} x[k] &= Ax[k-1] + Bu[k-1] && (2.11) \\ y[k] &= Cx[k] + Du[k] && (2.12) \end{aligned}$$

where, what x, y, u, A, B, C, and D stand for remain the same but they are defined at samples of k or k-1 instead of in continuous time.

2.6.1 State Space Modelling of 1 RC and 2 RC Circuits

State space equations are important while defining the model of a cell as an equivalent circuit. An equivalent cell circuit can be defined in a similar way to what is mentioned in Section 2.6. The inputs to the cell system can be the current that the cell is delivering or being charged with. The output of the cell system can be the terminal voltage that is observed at the terminals of the cell. The states of the system can be several, but the number of states required to fully represent the system must be equal to the order of the system.

In a cell, the SOC is a state that is of interest as described in Section 2.3. For the 1 RC model described in Section 2.5.2 the states can then be chosen to be I_{R1} and SOC (variable z where z is per unit SOC, i.e from 0-1). The equations that are important in the simulation environment are the discrete-time equations since the collection of data and simulations are done in discrete time and not continuous time. This will give state space equations in discrete time for 1 RC as

$$\begin{bmatrix} z[k] \\ I_{R1}[k] \end{bmatrix} = \begin{bmatrix} 1 & 0 \\ 0 & e^{\frac{-1}{R_1 C_1}} \end{bmatrix} \begin{bmatrix} z[k-1] \\ I_{R1}[k-1] \end{bmatrix} + \begin{bmatrix} \frac{\eta T_s}{3600Q} \\ 1 - e^{\frac{-1}{R_1 C_1}} \end{bmatrix} I[k-1] \tag{2.13}$$

where the variables have been described earlier in Section 2.5.2. The output equation is Equation 2.3 and in discrete time as

$$V_t[k] = OCV(z[k]) + I[k]R_0 + I_{R1}[k]R_1 \tag{2.14}$$

where the variables have already been defined in Section 2.5.2. It can be observed that Equation 2.14 cannot be directly written in the form of Equation 2.12. This is because Equation 2.14 is non-linear and specifically due to the OCV term which is non-linearly dependent on SOC (z).

Similar equations can be defined for the 2 RC model as

$$\begin{bmatrix} z[k] \\ I_{R1}[k] \\ I_{R2}[k] \end{bmatrix} = \begin{bmatrix} 1 & 0 & 0 \\ 0 & e^{\frac{-T_s}{R_1 C_1}} & 0 \\ 0 & 0 & e^{\frac{-T_s}{R_1 C_1}} \end{bmatrix} \begin{bmatrix} z[k-1] \\ I_{R1}[k-1] \\ I_{R2}[k-1] \end{bmatrix} + \begin{bmatrix} \frac{\eta T_s}{3600Q} \\ 1 - e^{\frac{-T_s}{R_1 C_1}} \\ 1 - e^{\frac{-T_s}{R_2 C_2}} \end{bmatrix} I[k-1] \tag{2.15}$$

where the variables are as it has been defined in Section 2.5.2. The output equation is Equation 2.6 and in discrete-time it is

$$V_t[k] = OCV(z[k]) + I[k]R_0 + I_{R1}[k]R_1 + I_{R2}[k]R_2 \tag{2.16}$$

where the variables have already been described in Section 2.5.2. The same as Equation 2.14 is observed about Equation 2.16, that it cannot be written as a linear output function in the state space representation due to the presence of the term OCV(z[k]).

2.7 Kalman Filter

Some of the states in a state space model are usually hidden and unavailable for measurement. In the example of the state space model of a 1RC and 2 RC circuit, it is the state of SOC and RC branch currents that are hidden and cannot be measured. A Kalman filter is implemented to estimate these hidden states. A Kalman filter is an algorithm that uses the data that can be measured about a system (using sensors for instance) to estimate the state vector x[k] of a system [14].

It is key to note that the Kalman filter uses measurements to estimate the states. Physical measurements are usually noisy and this must be taken into consideration when defining the equations of the system that will be fed to the Kalman filter. In addition, the definition of the system model might not be completely accurate and can have noise of its own. These two lead to a different definition of the model as compared to Equations 2.12 and 2.12. This new definition includes noises and is

$$x[k] = Ax[k-1] + Bu[k-1] + w[k-1] \tag{2.17}$$
$$y[k] = Cx[k] + Du[k] + v[k] \tag{2.18}$$

where, u[k] is a known, measurable input to the system, w[k] is the disturbance or process noise which signifies the lack of accuracy in our model, it has a covariance matrix of Σ_W and v[k] is the sensor noise in the output measurement, it has a covariance matrix of Σ_V. In the example of a 1 RC cell model, u[k] is the known current, w[k] is the process noise in determining the SOC and I_{R1} and v[k] is the noise that comes in during the voltage sensing of the terminal voltage.

When looking at the Kalman filter, the input to the filter is the system input, output measurement, past state estimates, and the system model. The filter then outputs estimates of the current states. In general, linear Kalman filters perform two main steps at each time step k [14], i.e. a prediction of the state and an estimation of it:

1. Prediction: The KF predicts the present state based on past data.

$$\hat{x}_k^- = A\hat{x}_{k-1}^+ + Bu_{k-1} \tag{2.19}$$

where the superscript $^-$ indicates a prediction and the superscript $^+$ indicates an estimation. The subscript $_k$ indicates that it is the current time step while $_{k-1}$ indicates that it is the previous time step. Hence, $\hat{x}_k^-$ signifies that the value is a current prediction and $\hat{x}_{k-1}^+$ signifies that the value is a previous estimation.

2. Estimation: The KF updates the prediction based on the knowledge it has from the measurement of the output and model. Therefore, for a KF to be effective the model should capture reality quite well. The prediction equation is

$$\hat{x}_k^+ = \hat{x}_k^- + L(y_k - \hat{y_k}) = \hat{x}_k^- + L(y_k - (C\hat{x}_k^- + Du_k)) \tag{2.20}$$

where L is the Kalman gain.

For systems where the equations 2.18 and 2.18 are linear, the linear Kalman filter can be used to predict the states. However, in cases where the system equations are non-linear as in a cell, non-linear Kalman filters such as the Extended Kalman Filter need to be used.

2.7.1 Extended Kalman Filter

An Extended Kalman filter is a version of the Kalman filter that can be used for solving non-linear systems. The non-linear system considered is

$$x_k = f(x_{k-1}, u_{k-1}, w_{k-1}) \tag{2.21}$$
$$y_k = h(x_k, u_k, v_k) \tag{2.22}$$

where the variables have been defined earlier in Section 2.7.

The EKF makes two main assumptions while solving the nonlinear model. For one, it assumes that the expectation of a function of variable x is approximately equal to the function of the expectation of the variable x. In mathematical terms

$$\mathbb{E}[f(x)] \approx f(\mathbb{E}[x]) \tag{2.23}$$

where $\mathbb{E}$ indicates expectation. Secondly, EKF linearizes the nonlinear system around the operating point by using Taylor expansion [15]. This means that the nonlinear system in 2.22 is expanded as a Taylor series around the prior operating point which is the set of values $(\hat{x}^+_{k-1}, u_{k-1}, \mathbb{E}[w_{k-1}])$. Thus as an example x_k would have a Taylor expansion as

$$x_k \approx f_{k-1}(\hat{x}^+_{k-1}, u_{k-1}, \mathbb{E}[w_{k-1}]) + \frac{\mathrm{d}f(x_{k-1}, u_{k-1}, w_{k-1})}{\mathrm{d}x_{k-1}}\bigg|_{x_{k-1}=\hat{x}^+_{k-1}} (x_{k-1} - \hat{x_{k-1}}^-) + \frac{\mathrm{d}f(x_{k-1}, u_{k-1}, w_{k-1})}{\mathrm{d}w_{k-1}}\bigg|_{w_{k-1}=\mathbb{E}[w_{k-1}]} (w_{k-1} - \mathbb{E}[w_{k-1}]) \tag{2.24}$$

which helps to linearize the error covariance time update.

The EKF follows similar main steps as the Kalman Filter, with the prediction and state estimation. However, the above-stated assumptions are made. The main steps of the EKF are indicated below [15].

The first step is the state prediction where the assumption regarding the expectation is made and the state is predicted as

$$\hat{x}^-_k = f(\hat{x}^+_{k-1}, u_{k-1}, \mathbb{E}[w_{k-1}]) \tag{2.25}$$

where all variables have the same meanings as in Equation 2.22 and $\mathbb{E}[w_{k-1}]$ is the expectation of the process noise and is often 0.

Values $\hat{A}_{k-1}$, $\hat{B}_{k-1}$, $\hat{C}_k$, $\hat{D}_k$ are found by linearizing the system around operating point $(\hat{x}^+_{k-1}, u_{k-1}, E[w_{k-1}])$ and are defined as

$$\hat{A}_{k-1} = \left.\frac{\mathrm{d}f(x_{k-1}, u_{k-1}, w_{k-1})}{\mathrm{d}x_{k-1}}\right|_{x_{k-1}=\hat{x}^+_{k-1}} \tag{2.26}$$

$$\hat{B}_{k-1} = \left.\frac{\mathrm{d}f(x_{k-1}, u_{k-1}, w_{k-1})}{\mathrm{d}w_{k-1}}\right|_{w_{k-1}=E(w_{k-1})} \tag{2.27}$$

$$\hat{C}_k = \left.\frac{\mathrm{d}h(x_k, u_k, v_k)}{\mathrm{d}x_k}\right|_{x_k=\hat{x}^-_k} \tag{2.28}$$

$$\hat{D}_k = \left.\frac{\mathrm{d}h(x_k, u_k, v_k)}{\mathrm{d}v_k}\right|_{v_k=E(v_k)} \tag{2.29}$$

where $\hat{A}_{k-1}$, $\hat{B}_{k-1}$, $\hat{C}_k$, $\hat{D}_k$ are non-linear system equivalents of A, B, C and D in linear systems in Equation 2.18 and Equation 2.18. These matrices are used to calculate the Kalman Gain L_k. The assumption on the expectation of a function is made again in estimating the system output estimate, $\hat{y_k}$. It is defined as,

$$\hat{y}_k = h(\hat{x}^-_k, u_k, \mathbb{E}[v_k]) \tag{2.30}$$

where $\mathbb{E}[v_k]$ is the expectation of the sensor noise, $\hat{x}^-_k$ is the prediction made in Equation 2.25.

The Estimation step of the EKF follows the same way as the linear Kalman filter as

$$\hat{x}^+_k = \hat{x}^-_k + L_k(y_k - \hat{y_k}) \tag{2.31}$$

where $\hat{y_k}$ is the system output estimate found in Equation 2.30.

Chapter 3

Testing

This chapter covers the testing phase of the thesis. The test object, i.e. the lithium-ion cell tested is presented and the key data of the cell is presented. The test methodology is designed and described and each specific test conducted is presented. In addition, all of the equipment used in the tests is presented.

3.1 Test Object

Within the scope of the thesis was also the collection of data from cells that were then to be used to model the cell and to validate the accuracy of the model and the estimation algorithms. For this purpose, Li-ion cells were tested in the Chalmers Battery Lab. The cells chosen for testing were commercially available cylindrical cells from the company LG Chem. The cell product number was INR18650MJ1. The relevant specifications of the cell are given in Table 3.1 [16].

Figure 3.1: Image showing the test object

Table 3.1: Cell specifications of cell INR18650MJ1

Item	Condition	Specification
Nominal Voltage		3.635 V
Nominal Capacity		3500 mAh
Standard Charge	Constant Current Constant Voltage Cut-off Current	0.5C (1700 mA) 4.2 V 50 mA
Standard Discharge	Constant Current Cut-off voltage	0.2C (680 mA) 2.5 V
Max Charge Current		1C (3400 mA)
Max Discharge Current		10 A

3.2 Design of Test Methodology

The end goals for the usage of the data were kept in mind while determining the type of tests that were to be done. The testing was divided into two types - Reference Performance Tests (RPT) and Dynamic Testing.

As the name suggests, the Reference Performance Tests were used to characterize the cell reference parameters such as the cell impedance, cell capacity, and OCV versus SOC characteristics. Then Dynamic Testing was performed to mimic the functioning of the cell in the real world in electric vehicle applications. The Worldwide Harmonised Light Vehicles Test Procedure (WLTP) was followed during the dynamic testing of the cell. The speed profile of the WLTP cycle was scaled to have the 1C current specified for the cell (in this case 3400 mA) as its RMS current value as shown in Figure 3.3. The cell discharge current was then chosen to be this current profile. The RPT was the series of tests performed at the beginning of the testing procedure. After the RPT a certain number of Equivalent Full Cycles (EFC) of dynamic testing were performed after which the RPT was repeated. This general testing flow is shown in Figure 3.2.

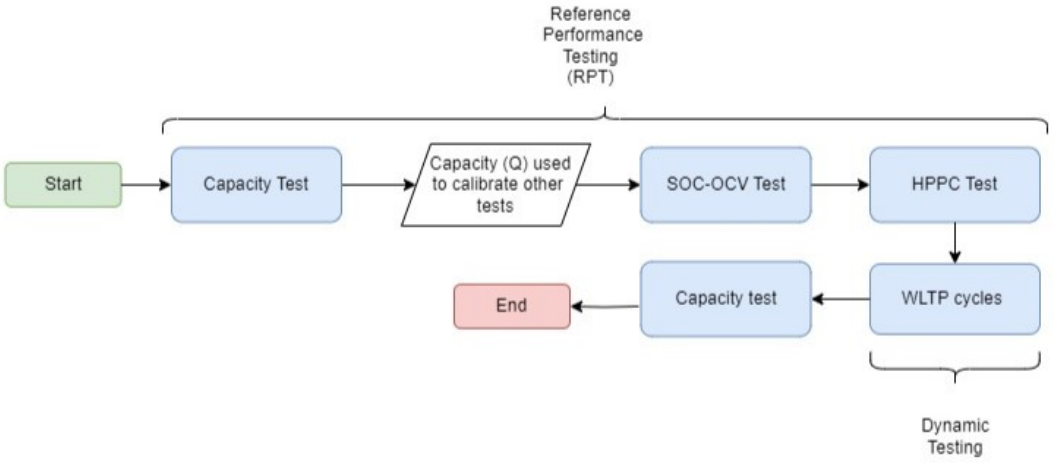

Figure 3.2: Flowchart showing the testing procedure

3.2.1 Reference Performance Tests (RPT)

The three types of RPT performed during the thesis were the Capacity Test, HPPC Test, and SOC-OCV relationship establishment.

1. **Capacity Test**

The Capacity test was used to find the charge and discharge capacity of the cell and was performed at 25°C. The datasheet suggested charging of the cell followed by the discharging and hence this procedure was followed. First, the cell was discharged to 2.5V so the procedure could be initialized. Then it was allowed to rest in an idle state for 30 minutes. Following this, the cell was charged following the Standard Charge procedure. This involved charging at a constant current of 0.5 C (1700mA) till the cell voltage reached 4.2 V. Then the charging switched to constant voltage mode at 4.2 V and the current tapered down. The charging was terminated when the current had tapered down to 50 mA. The charge capacity of the cell is the Ah of charge put into the cell during this entire charge procedure.

Following the charge capacity test, the cell was allowed to rest in an idle state for 30 minutes. Then the discharge procedure was started. The Standard Discharge process involved a constant current discharging from 4.2 V to 2.5 V. The charge in Ah that was discharged from the cell during this discharge step gives the discharge capacity of the cell. The discharge capacity of the cell was the quantity that was used further as the Capacity of the Cell. This value was used to calibrate the different SOC windows. The ratio of the discharge to charge capacity was also used to yield the useful quantity of Coulombic efficiency (η).

2. **Hybrid Pulse Power Characterization (HPPC) Test**

This test was performed to obtain data that can be used to capture and then characterize the dynamic behavior of the cell by calibrating the cell parameters such as impedance. The test consisted of charge and discharge pulses at different SOC levels. In the test procedure, the current pulses were applied at every 10 % step of SOC. The procedure followed for the HPPC test was as follows:

i. The cell is charged up to 100 % SOC through the Standard Charge Procedure.

ii. The cell rests in an idle state for 60 minutes.

iii. A discharge pulse of 1C (3400 mA) is applied for 10 seconds.

iv. The cell rests in an idle state for 10 minutes during which time relaxation of the open circuit voltage occurs.

v. A charge pulse of 1C (3400 mA) is applied for 10 seconds.

vi. The cell rests in an idle state for 10 minutes.

vii. The cell is discharged by 10 % SOC to the next SOC level. This 10 % is determined as the 10 % of the discharge capacity found from the Capacity test.

viii. Step ii-vii are repeated 9 more times such that the future pulses are applied at 90 % SOC, 80 % SOC, and so on till 10 % SOC.

3. **SOC-OCV Relationship**

The SOC-OCV relationship was necessary to build a model of the cell. However, the only voltage accessible was the terminal voltage. When the cell is allowed to rest in an idle state for a long time the cell terminal voltage tends to the open circuit voltage of the cell. However, performing this at every level of SOC is time-consuming since it involves a small discharge or charge followed by a long duration of rest. So instead, a pseudo-SOC-OCV test was conducted. This involved charging and discharging at $\frac{1}{10}$ C current.

3.2.2 Dynamic Testing

In total 8 cells were used for dynamic testing. They were divided into 4 groups with 2 cells in each. The cells in each group were dynamically cycled between different SOC windows. The SOC windows assigned to each group are presented in Table 3.2.

Table 3.2: SOC windows used for cycling

Group	SOC Window	Cycles giving 100 EFC
Group 1	(0-100) %	100
Group 2	(25-100) %	133.3
Group 3	(50-100) %	200
Group 4	(25-75) %	200

An Equivalent Full Cycle (EFC) is said to have occurred when capacity equal to the capacity of the cell has been charged and discharged. Hence 1 EFC is 1 charge and discharge cycle in the (0-100) % SOC window but 2 charge and discharge cycles in the (50-100) % SOC window. The initial aim was to test at different temperatures to imitate the changing seasons. However, due to time constraints, the tests were limited to 25 °C. In addition, only the 1C (rms) current profile of WLTP was used, as shown in Figure 3.3. 1C (rms) current means that the root-mean-square value, of the dynamic WLTP current, is equal to the 1C current of the cell, i.e. 3.4 A.

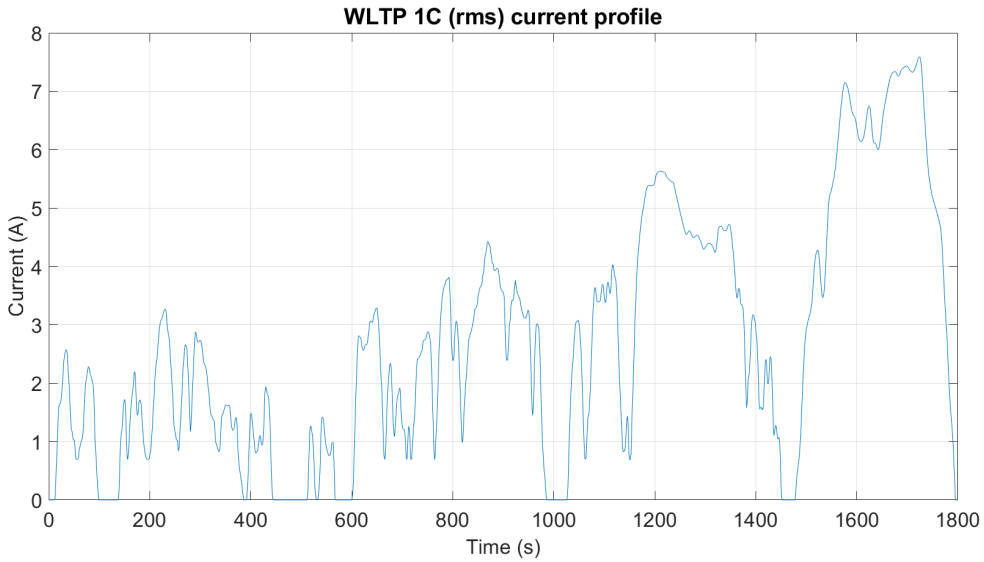

Figure 3.3: WLTP current profile for 1C (rms) current

3.2.3 Complete Test Procedure

The complete test procedure consisted of the RPT (that consists of the 3 tests specified in Section 3.2.1), followed by 100 EFC of dynamic testing, followed by RPT, followed by 50 EFC, followed by RPT, followed by 50 EFC, followed by a capacity test. This is shown in Figure 3.4 to be understood more concisely.

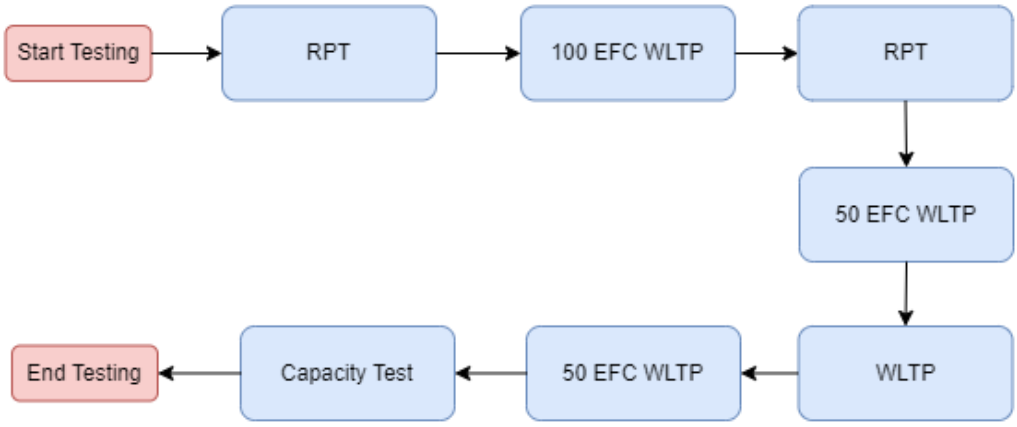

Figure 3.4: Complete testing procedure

In Figure 3.5 the voltage, current, and charge-discharge capacities are shown during different tests. The section marked 1 in the figure are the 2 initial capacity tests. Section 2 is the pseudo-OCV-SOC test. Section 3 is the HPPC test, Section 4 is the

WLTP dynamic cycling (only 5 WLTP cycles are pictured here for ease of visualization) and this is followed by another capacity test.

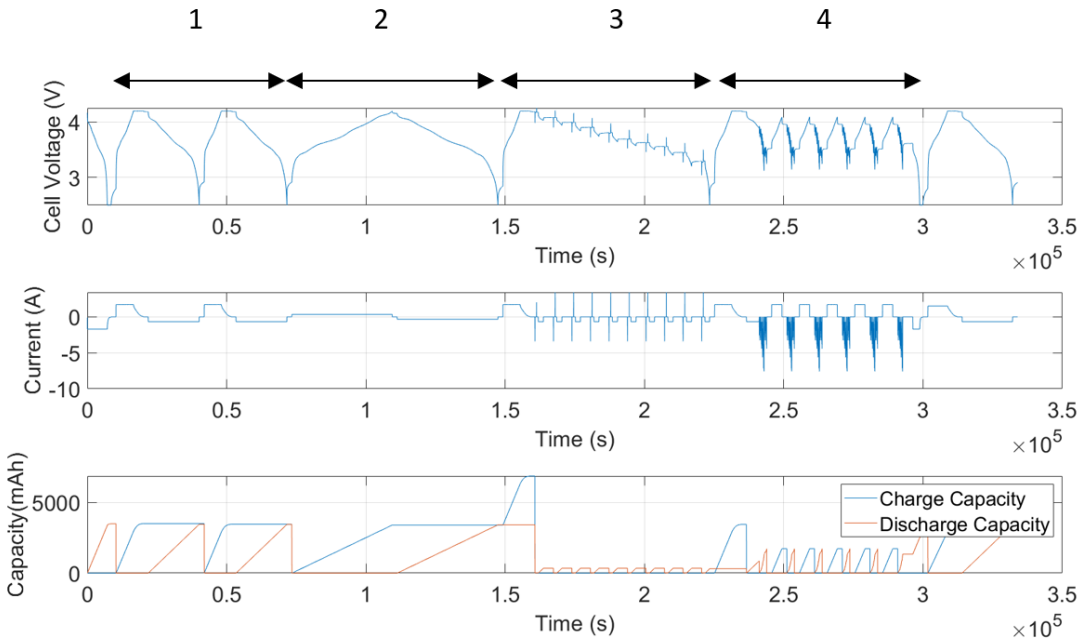

Figure 3.5: Cell measurements and calculations during complete testing procedure

3.3 Equipment Used During the Testing

In this Section, the test equipment used during all tests is presented. This equipment was located in the Chalmers Battery lab.

3.3.1 Test Rig Preparation

As part of the thesis, connections were prepared between the wiring harness and the cell holder. Some connections were prepared by soldering and others by crimping. The labeled result is presented in Figure 3.6. The voltage sense sensed the terminal voltage. The power cables were used to feed in the current and the positive current was the charging current. A temperature sensor was attached to the body of the cell to monitor the temperature.

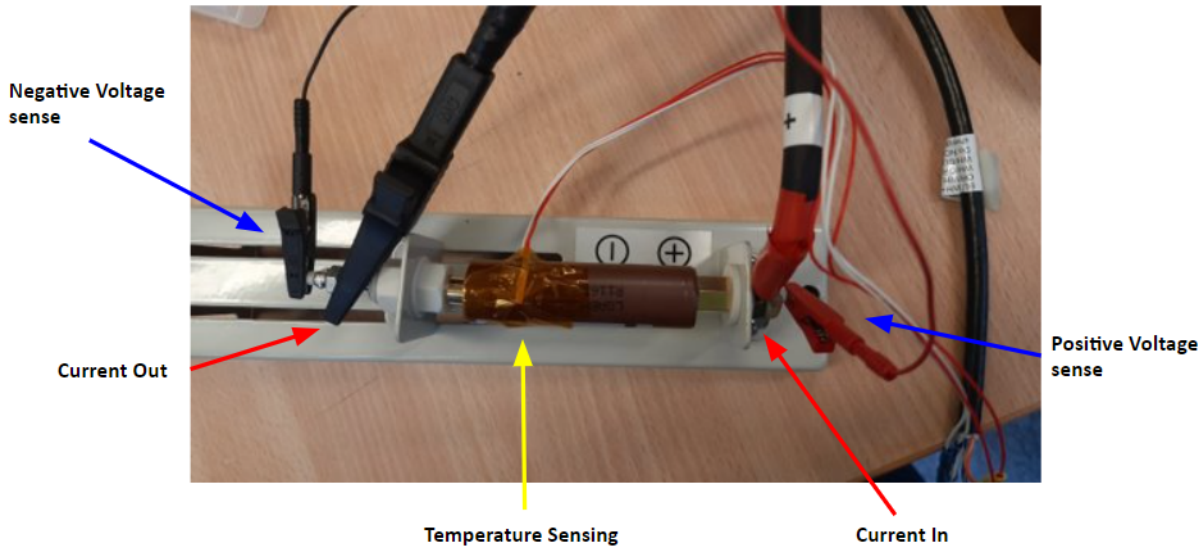

Figure 3.6: Testing set-up

3.3.2 Cell Tester and Programming

The cell tester used to cycle the cell and control the currents to it was an Advanced Cell Tester (ACT) from the company PEC. The cycler has several channels and 8 of them were used for the thesis, one for each cell. This Cycler was controlled via the MWare software on the host computer. In the MWare software, a script of tests was created to contain all the tests that were described in Section 3.2. Figure 3.7 shows a picture of the PEC ACT and the different channels can be observed. The cell tester records the current, temperature, voltage, and other quantities every second, so the time sample of the data collected is 1 second. Some important specifications of the Cell tester are listed in Table 3.3. Figure 3.8 shows an example of script writing in the MWare Software. The same software allows one to run the tests, pause the tests, and plot the test data in real-time. After the tests were complete Result Inspection software was used to collect and visualize the data. The same software can be used to export the test data for later analysis.

Table 3.3: PEC cell tester specifications

Item	Specification
Sampling frequency	1 Hz
Voltage sensor range	0 V - 5 V
Voltage sensor resolution	1.9 μV
Current sensor range	0 A - 50 A
Current sensor resolution	8 μA

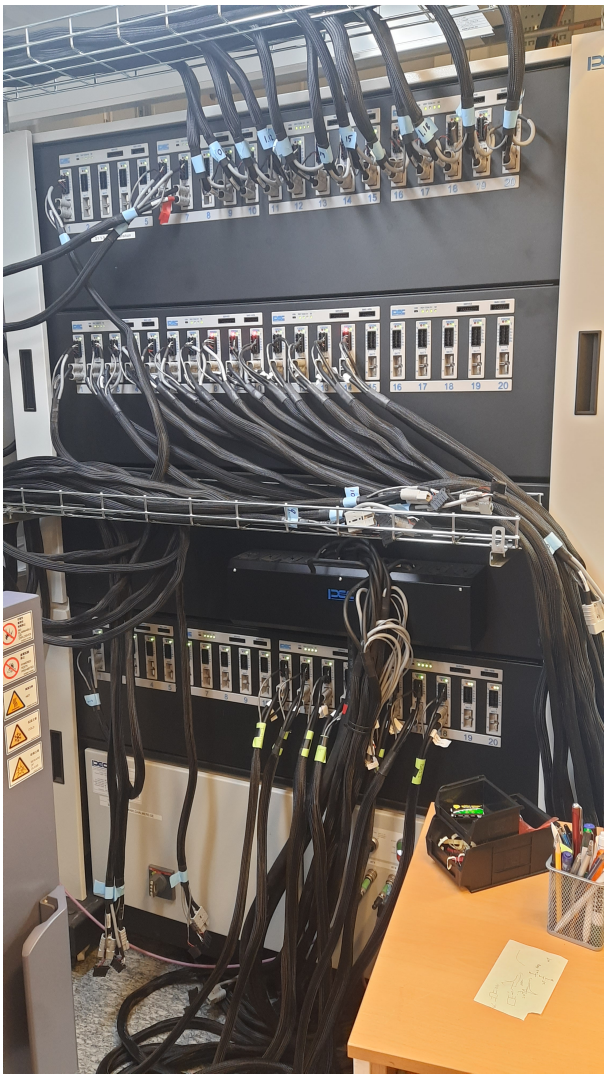

Figure 3.7: PEC advanced cell tester

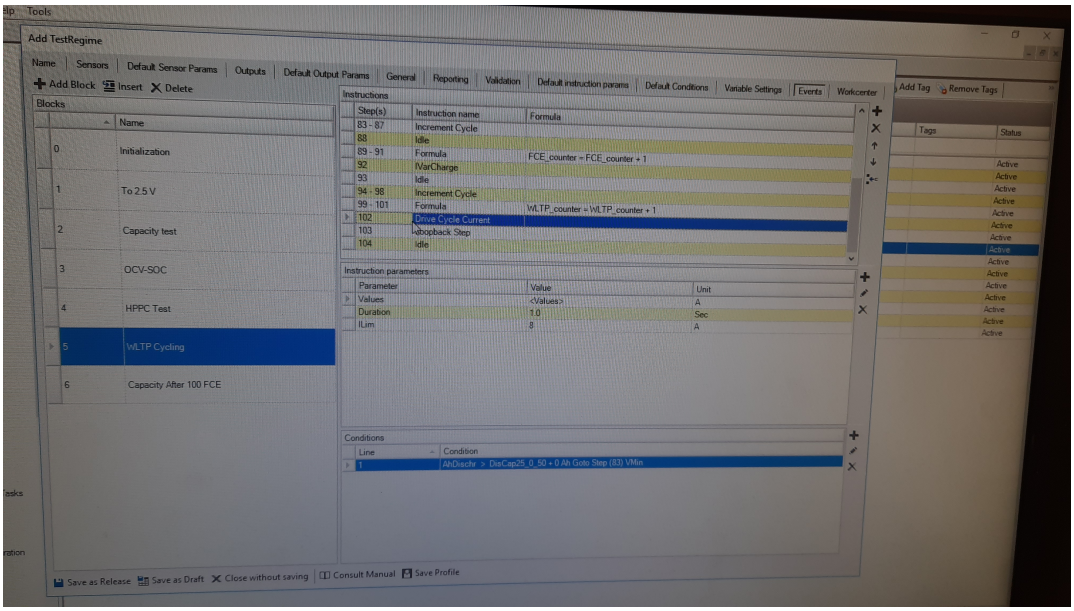

Figure 3.8: Scripting the tests in Mware on the host computer

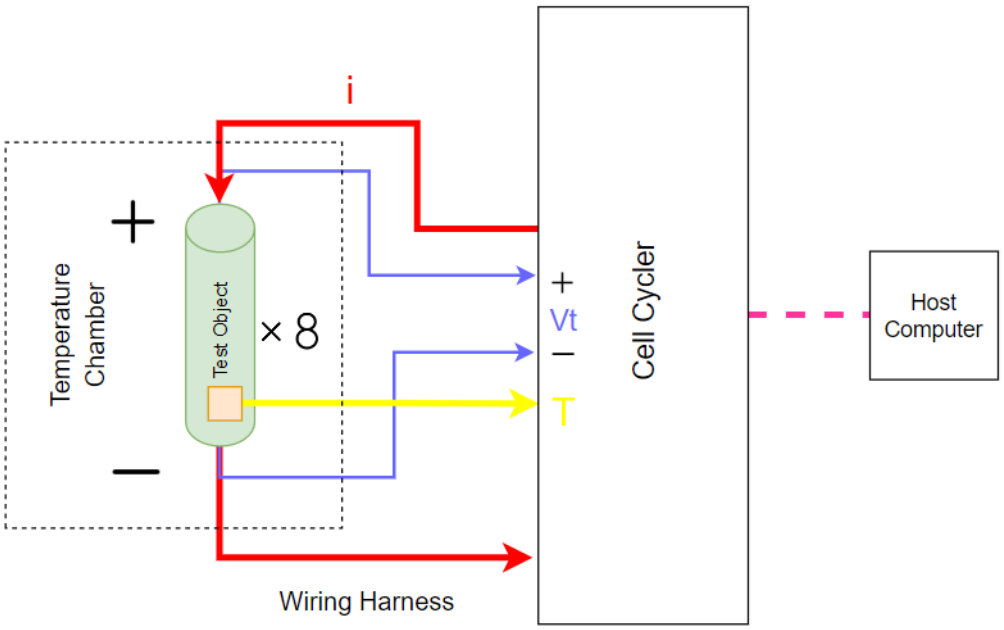

Figure 3.9: Testing set-up

3.3.3 Temperature Chamber

To maintain the temperature at 25°C throughout the testing, a temperature chamber was used. The cell holders were placed within the chamber and the temperature chamber had an opening through which the wiring harness could be carried out and to the cell cycler. The temperature chamber used was from the company ESPEC and can be

seen in Figure 3.10. It was capable of controlling both temperature and humidity but the humidity function was not used in the thesis.

Figure 3.10: Temperature chamber

Chapter 4

Modelling

This Chapter presents the methodology followed in modeling using the data obtained as described in Chapter 3. First, the pre-processing of test data and obtaining of the SOC-OCV curves is described. This is followed by methods used to obtain the model parameters from the test data. Finally, the 1 RC and 2 RC modeling done in the MATLAB Simulink simulation environment is presented.

4.1 Pre-processing of Testing Data

Before the data was ready to be used it had to undergo some processing. One of the main reasons for this was that the cell tester generally sampled the data at 1-second intervals but whenever there was a change in the step in the script, for instance, if the test went from constant current charging to constant voltage charging, the cycler would sample data at a rate faster than 1 second. Since the model was to be built in discrete-time, handling data with varying sampling times would be tricky so it was decided to filter the data. This filtering led to some loss of data, such as some sharp peaks. The method was to round down all the time steps retaining only the first time step and discarding the data for the duplicates. For instance, if there was data at times 10.01s, 10.3s, and 10.99s only the data from 10.01s was retained.

4.2 Identification of SOC-OCV Lookup Table

To identify the SOC-OCV lookup table, the results from the SOC-OCV test were used. It is worth mentioning that the SOC-OCV test was a pseudo-SOC-OCV test. This meant that the voltage obtained was not the true OCV but contained a voltage drop or gain (IR drops) due to internal resistance based on whether the cell was being discharged or charged. Since the charge and discharge current were very low during this test, the voltage drop or gain was also small but could still lead to some significant errors in the model. Thus it was necessary to compensate for this. The method described in [12] was used to identify the true OCV from the pseudo-OCV.

The measured charge OCV is higher than the measured discharge OCV as shown in Figure 4.1. The true charge OCV is lower than the measured and the true discharge

OCV is higher than the measured. Just as the charging starts (i.e. current goes from zero to non-zero), the terminal voltage goes up by a value equal to the voltage gain. When the charging stops (current goes to zero again), the terminal voltage falls by a value that was the voltage gain just before that instant. The method assumes that the voltage gain varies linearly between these two voltage gains, this means assuming the internal resistance varies linearly between the two SOCs since the current was kept constant. Then this linear array was subtracted from the measured OCV to get the IR-drop-compensated charge OCV. This is presented in Section 6 in Figure 6.3.

Just as the discharging starts (i.e. current goes from zero to non-zero), the terminal voltage goes down by a value equal to the voltage drop. When the discharging stops (current goes to zero again), the terminal voltage goes up by a value of the voltage drop just before that instant. The method assumes that the voltage drop varies linearly between these two voltage drops, this means assuming the internal resistance varies linearly between the two SOCs since the current was kept constant. Then this linear array was added to the measured OCV to get the IR-drop-compensated discharge OCV. This is presented in Section 6 in Figure 6.3.

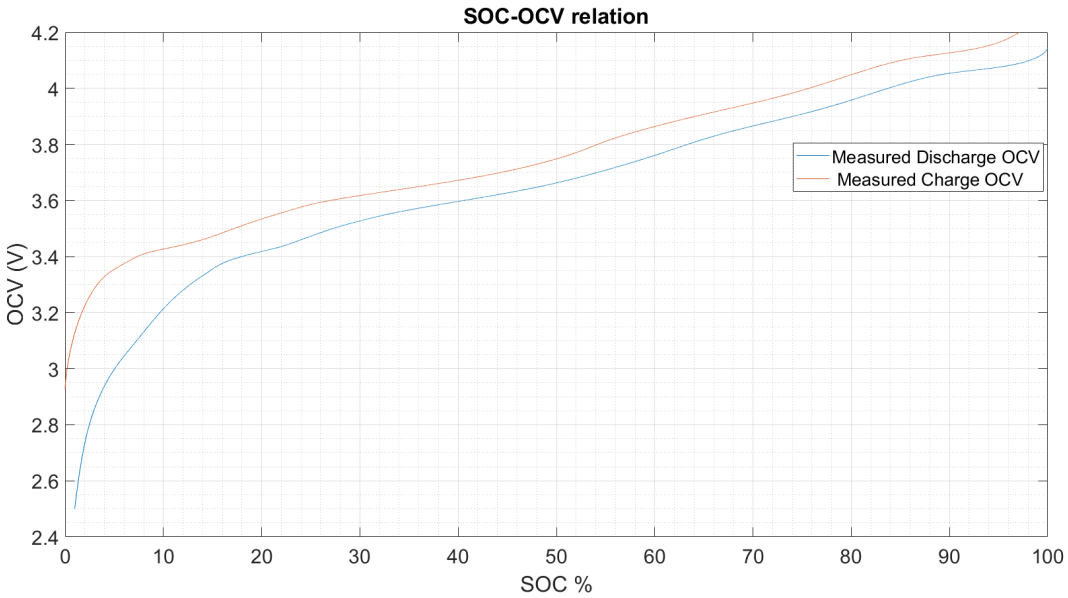

Figure 4.1: Measured OCV during (pseudo) OCV-SOC test

Since the discharge process was cut-off at 2.5 V the cell did not reach 0 % SOC during discharge. During charge, the current is cut off when cell voltage reaches 4.2 V and there is no constant voltage charge following this. Hence the SOC does not reach 100 % during charge. Due to this in Figure 6.3 it is seen that the discharge and charge curves alone do not cover the entire SOC range. To solve this a method presented in [12] was used. This involves using the charge OCV between (0-50) % SOC and using the discharge OCV between (50-100) % SOC. The way this was done is that at 50 % SOC, the difference in the IR compensated charge and discharge OCV curves is found and the averaged OCV curve must pass exactly in between the two curves. Then from (0-50) % SOC the charge OCV curve has a value subtracted from it such that at 0 % SOC the curve stays at the same point but at 50 % it moves down by half the

difference between the curves. At all the SOCs in-between the OCV is brought down by an amount proportional to the SOC, i.e. at 40 % SOC the OCV is brought down by 0.4 x (difference between the curves). The discharge curve is brought up in the same way in the (50-100) % range. The resulting curve is presented in Section 6 in Figure 6.4.

Thus two OCV-SOC look-ups were identified. One in which the charge or discharge condition was taken into consideration by looking at the sign on the current (positive meant charge and negative meant discharge) and a look-up was based on that. For the SOCs which had data missing the curve was linearly interpolated. The other look-up possible was a single one that was used throughout and was the averaged SOC-OCV look-up table.

4.3 Obtaining Parameters

Before the cell model was implemented, an estimate of the initial values of the cell parameters was required. This meant calculating from the test data the values of R_0, R_1, C_1, R_2 and C_2. The results from the HPPC test were used for this purpose. Two different methods were attempted in this thesis for the 1 RC circuit. One was using the physical interpretation of the circuit component values and another was using a built-in optimization tool in MATLAB. Only the MATLAB optimization technique was used for the 2-RC circuit. The results are presented later in Section 6 however the technique is presented here.

1. Using Physical Interpretation of 1 RC Values

The values of R_0. R_1 and C_1 were found by following the physical interpretation in Figure 4.2 and applying it to the HPPC curve that was found from the test data as shown in Figure 4.3 [12]. Since the HPPC pulses were provided at 10 different SOC levels the values of the parameters were possible to be found at different SOCs. At intermediate SOC levels, the resistance was assumed to stay the same. It can be seen from Figure 4.2 that there could be found three equations and these could be solved to provide three unknown parameters.

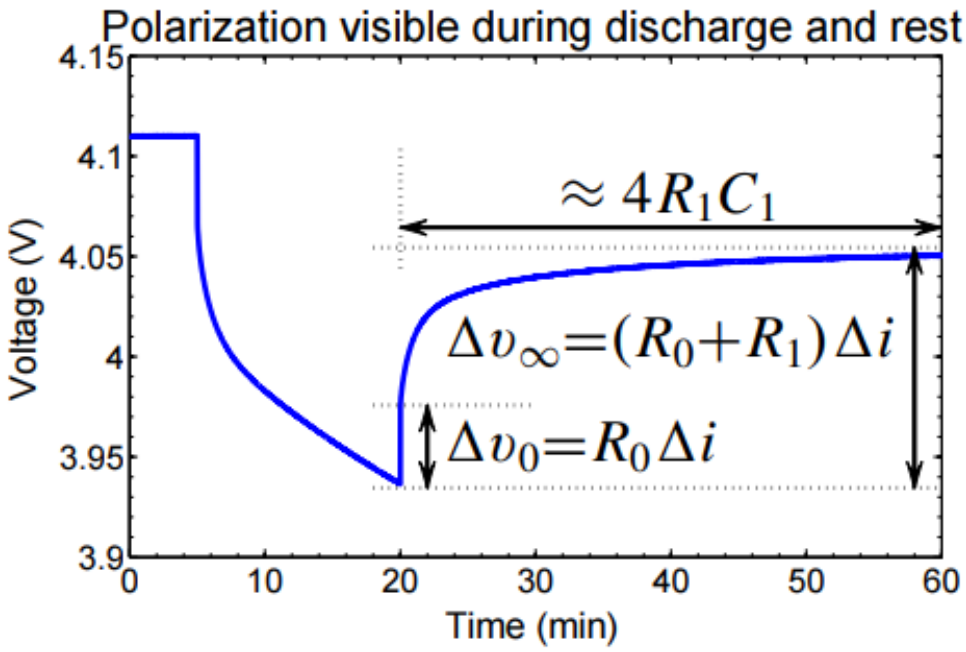

Figure 4.2: Physical calculation of R_0, R_1 and C_1 method

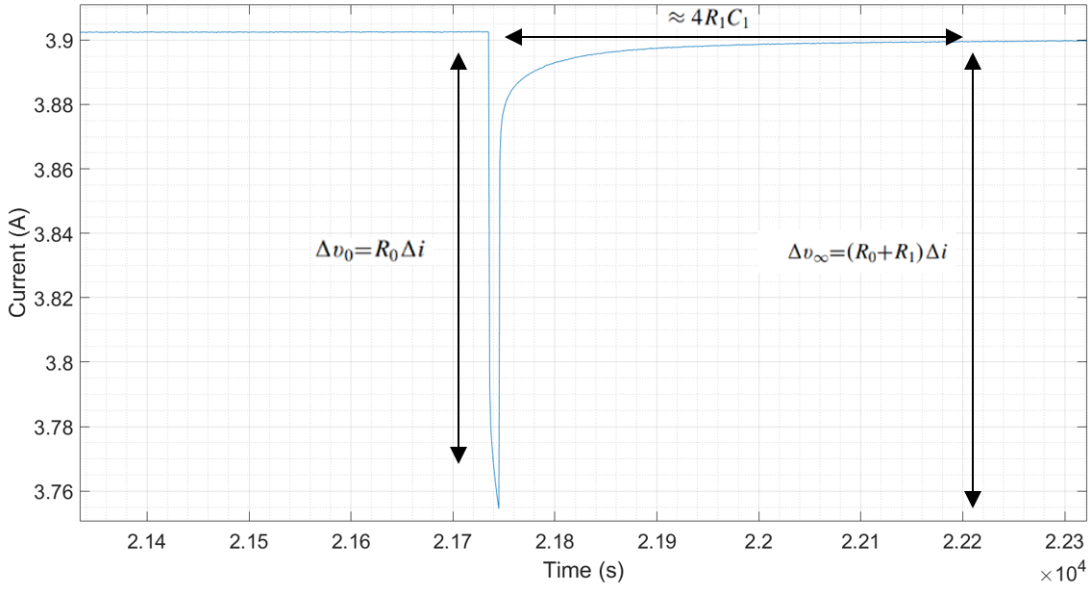

Figure 4.3: Physical calculation of R_0, R_1 and C_1 method applied to HPPC data

2. The second method involved using a built-in optimizer in MATLAB. More details regarding this method can be found in [17] but the steps are mentioned here briefly. Both the outputs of the model as well as experimental results were loaded into the MATLAB workspace. Then the Parameter Estimation App (Part of Simulink Design Optimization) was opened. A New Experiment was created with the names of the model output entered as well and the experimental data was selected in the time duration needed (in this case it was the HPPC pulse). Then the parameters to be estimated in the model were chosen. Then the parameters were estimated. The estimation was

done through iterations and once the values reached a steady state the process could be stopped and the values noted down. When the optimization was done at the 10 different SOCs between 0%-100% at which the HPPC pulses were applied, the parameter values were optimized for 10 levels of SOC. Figure 4.4 shows the screen of the Parameter Estimation Application. The default optimization method and algorithm were used. The application by default uses the Nonlinear least squares method of optimization and the Trust-region-reflective algorithm.

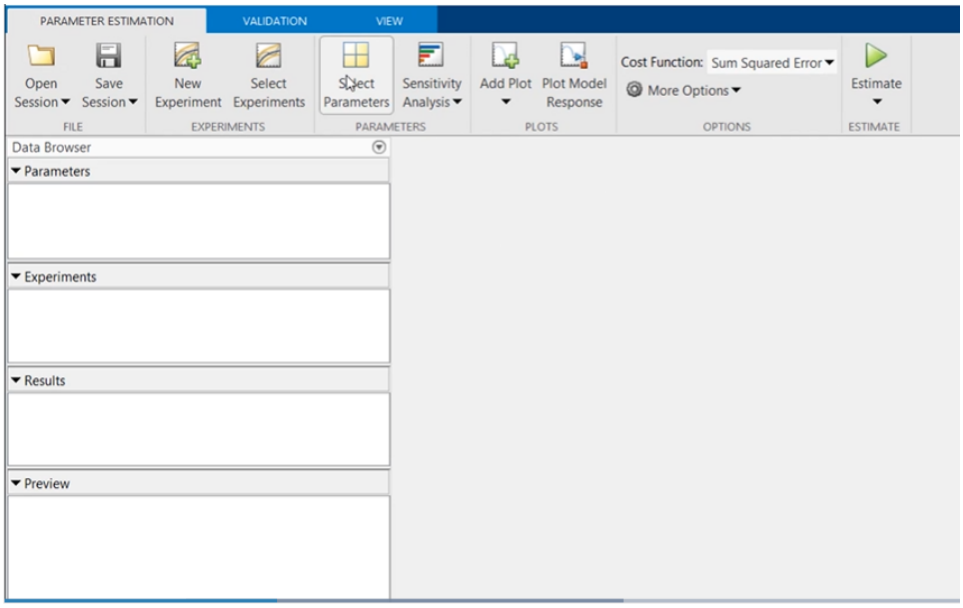

Figure 4.4: Interface of the MATLAB parameter estimation application

4.4 1 RC and 2 RC Modelling

While building the RC model in MATLAB, there were some considerations made. There were options for different parameters based on the method they were obtained - through the optimizer or the physical interpretation. The different OCV curves were used to determine which OCV-SOC curve modeled the cell the best. The OCV curve combinations that were tried were - the blended OCV described in Section 4.2, the charge and discharge OCV compensated for IR drop, and the charge and discharge OCV as obtained from the test but with a fixed offset included.

The equations of the model were formed as previously stated in Section 2.6.1. There were again different ways to implement the state space models in Simulink. One possible method was to use the discrete-time state space models readily available in Simulink as shown in Figure 4.5. However, this model was found to provide limited tunability when it came to the usage of different parameter values based on the SOC value, i.e. the A and B matrices and output equation was not time-invariant but rather depended on the SOC which changed with time. Thus it was better to make a function implementation that took the SOC as an input and used it to compute the parameters and then the new A and B matrices and output. This is demonstrated in Figure 4.6.

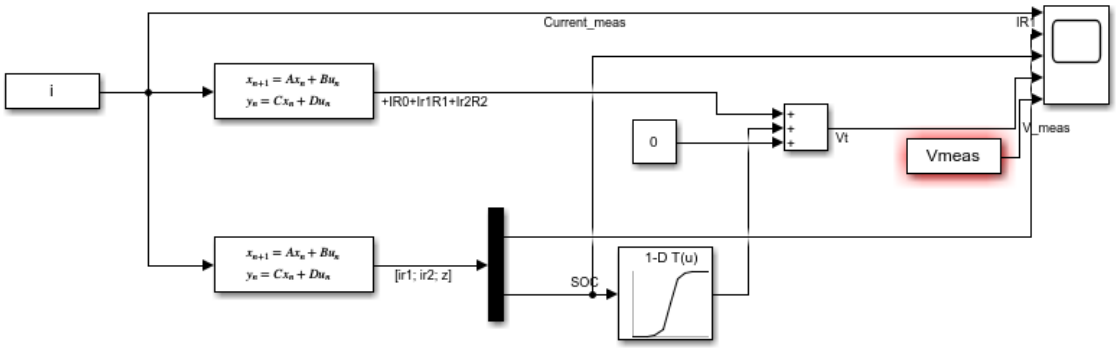

Figure 4.5: Simulink built-in block for cell model implementation

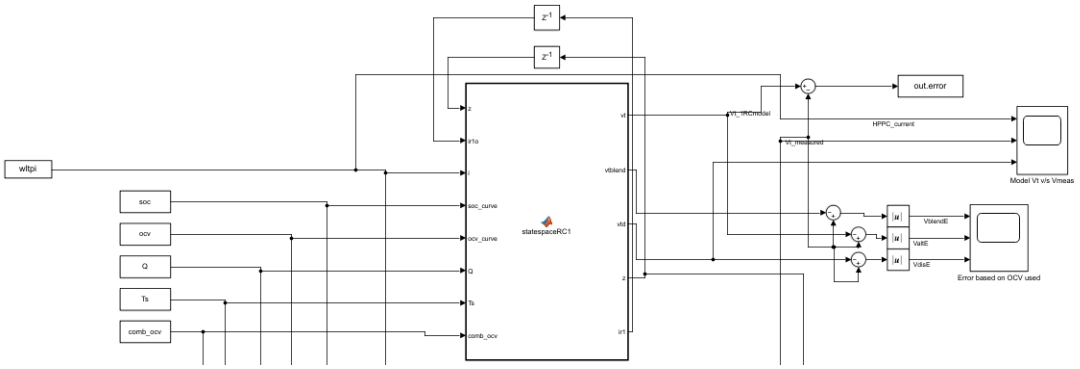

Figure 4.6: Function block development in Simulink for cell model implementation

Once the best combination of OCV-SOC curve, parameters, and type of model was secured for the 1 RC circuit the same was used for the 2 RC circuit. The 2 RC circuit was then implemented similarly, with the only difference being the usage of an additional equation to describe a state.

Since the parameters were calculated using the HPPC curve there would not have been much significance in validating the model against the HPPC curve. However, it was done to obtain an idea of how well the model fits the HPPC data. The model was then validated against the WLTP dynamic cycling as this would be an actual use case in the real-world scenario.

Chapter 5

State Estimation

Once the cell model was implemented in MATLAB and its accuracy checked, the state estimation using Kalman filters could be implemented. As noted before, the Kalman filter is most useful when the system model is accurate. Thus, it was necessary to build, understand, and improve the system model before implementing state estimation algorithms on it. It was decided after modeling to proceed with the 1RC model. The motivation behind this decision is described in Chapter 6, but the model used in this chapter is only the 1RC model.

5.1 SOC Estimation with Fixed Parameters in Extended Kalman Filter

To start the state estimation, first, the parameters of the cell model such as R_0, R_1, and C_1 were assumed to change with SoC as was found in Section 4.3 and found for intermediate values using interpolation. The cell capacity was assumed to remain constant to simplify the process. The only states being estimated by the Kalman filter were the SOC and current through R_1. This meant that the state matrix x could be written as

$$x = \begin{bmatrix} z \\ i_{R1} \end{bmatrix} \tag{5.1}$$

where all variables hold the same meaning as previously described. The steps followed in the algorithm were adapted from [15]. The steps are described below:

1. The parameters of the cell model R_0, R_1, and C_1 were linearly interpolated based on values found from test data.

2. The matrices $\hat{A}_{k-1}$ and $\hat{B}_{k-1}$ were computed as shown in Equation 2.27 and Equation 2.28. For a 1RC model as depicted in Equation 2.13 the matrices $\hat{A}_{k-1}$ and $\hat{B}_{k-1}$ were

$$\hat{A}_{k-1} = \begin{bmatrix} 1 & 0 \\ 0 & e^{-\frac{T_s}{R_1 C_1}} \end{bmatrix} \tag{5.2}$$

$$\hat{B}_{k-1} = \begin{bmatrix} 1 & 0 \\ 0 & 1 \end{bmatrix} \tag{5.3}$$

where all variables hold the same meaning as previously described.

3. The state estimate was time updated as in Equation 2.25. For a 1RC circuit, this state update was done using the system equation as described in Equation 2.13 and was

$$\hat{x}_k^- = \begin{bmatrix} 1 & 0 \\ 0 & e^{\frac{-T_s}{R_1 C_1}} \end{bmatrix} \hat{x}_{k-1}^+ + \begin{bmatrix} \frac{\eta T_s}{3600Q} \\ 1 - e^{\frac{-T_s}{R_1 C_1}} \end{bmatrix} u_{k-1}^- \tag{5.4}$$

where all the variables have the same meanings as described previously.

4. The error covariance matrix was time updated. It used the previous value of the matrix and the values of $\hat{A}_{k-1}$ and $\hat{B}_{k-1}$. It was calculated as

$$\Sigma_{X,k}^- = \hat{A}_{k-1} \Sigma_{X,k-1}^+ \hat{A}_{k-1}^T + \hat{B}_{k-1} \Sigma_W \hat{B}_{k-1}^T \tag{5.5}$$

where $\Sigma_{X,k}^-$ is the covariance matrix of the error in the state estimation and Σ_W is the covariance matrix of the process noise w.

5. The matrices $\hat{C}_k$ and $\hat{D}_k$ were found as described in 2.29 and 2.29. For a 1 RC circuit, this was found to be

$$\hat{C}_k = \begin{bmatrix} \left.\frac{\mathrm{d}OCV}{\mathrm{d}z}\right|_{z=z_k^-} & R_1 \end{bmatrix} \tag{5.6}$$

$$\hat{D}_k = 1 \tag{5.7}$$

where $\frac{\mathrm{d}OCV}{\mathrm{d}z}$ is the rate of change of the OCV voltage with respect to SOC at the SOC (z_k^-) time update in Step 3.

6. The system output was estimated for a 1RC model as

$$\hat{y} = V_{ocv} + R_1 \hat{x}_k^-(2,1) + R_0 u_{k-1}^- \tag{5.8}$$

where $\hat{x}^-(2,1)$ is the time update estimate of the current through the resistor of the RC branch in the 1RC model.

7. The Kalman gain matrix was computed using the matrices computed in the previous steps. It took into consideration the system process noise and the sensor noise as well as the system and output equations in the model. Thus giving an optimal value for L. It was computed as

$$L = \frac{\Sigma_{X,k}^{-} \hat{C}_k^{\,T}}{(\hat{C}_k \Sigma_{X,k}^{-} \hat{C}_k^{\,T} + \hat{D}_k \Sigma_V \hat{D}_k^{\,T})} \tag{5.9}$$

where the variables are the same as defined previously.

8. The state estimate $\hat{x_k}^-$ was updated based on the measurement of the output, y from the sensor and using the Kalman gain, L, computed in step 7. This was computed as

$$\hat{x}_k^+ = \hat{x}_k^- + L(y - \hat{y}) \tag{5.10}$$

where y is the measured cell terminal voltage in volts and the other variables remain the same as previously defined.

9. With the computed Kalman filter gain, L, an update was also made on the error covariance matrix Σ_X as

$$\Sigma_{X,k}^{+} = \Sigma_{X,k}^{-} - L\hat{C}_k \Sigma_{X,k}^{-} \tag{5.11}$$

where $\Sigma_{X,k}^{+}$ is the measurement updated error covariance matrix and is fed back to the Kalman filter in the next step as $\Sigma_{X,k-1}^{+}$.

The above-described 8 steps gave a state estimate from the Kalman filter. They were implemented in MATLAB Simulink environment using a MATLAB function block with the desired inputs and outputs as shown in Figure 5.1. The figure shows the inputs to the function which were 'xhat' and 'SigmaX' which were fed back from the function through a unit delay, 'SigmaW' and 'SigmaV' which were tuned manually in the script to the best estimates of the process and sensor noise, 'input_i' and 'ytrue' which were data processed from the test on the cell current and terminal voltage, the 'soc_curve' and 'ocv_curve' which was the SOC-OCV data that was processed from the test data, Q which was the cell capacity, assumed constant at this point and Ts which was the sample time which was 1 second in this case. The words appear as they do in the text above because they are referencing the variable names that were given in MATLAB. For example, the 'xhat' variable in MATLAB references $\hat{x}$.

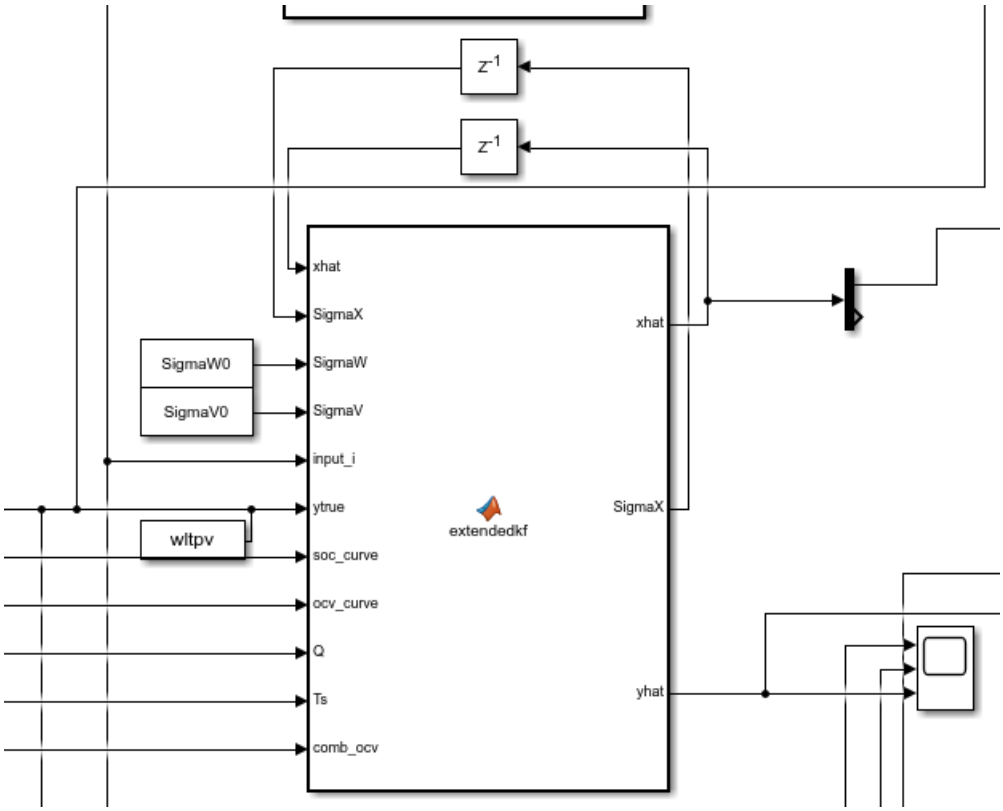

Figure 5.1: Extended Kalman filter implemented in Simulink

5.2 Joint Extended Kalman Filter

As noted in Section 2.5.2 and Section 2.3.1 the values of parameters R_0, R_1, C_1, and the capacity Q change over time. They however change much slower than the value of the states previously estimated, i.e. SOC and I_{R1}. The variation of the parameters R_0, R_1, C_1, and Q can be estimated to be very slow and negligible. They are assumed to be almost constant but a small noise is added to them, this is to ensure that these values can still change over time. The method followed to implement the JEKF can be found in [18]. Thus if we consider any of the parameters to be θ, we see a variation as

$$\theta_k = \theta_{k-1} + w_{k-1} \tag{5.12}$$

where w_k is modeling the addition of noise or small variations to the parameter θ_k and has the covariance of Σ_W.

5.2.1 JEKF for Parameter Estimation

The Joint extended Kalman filter was designed to estimate over time the values of the SOC, i_{R1}, R_1, C_1, and R_0. Since only small variations are allowed in R_1, C_1, and R_0, it is important to initialize them close to the actual value. This is done using the results of the tests performed as described in Chapter 3 and the parameters extracted as described in Section 4.3.

The system and output equations for the joint extended Kalman filter now became:

$$
\begin{aligned}
x[k] &= \begin{bmatrix} z[k] \\ i_{R1}[k] \\ R_0[k] \\ R_1[k] \\ C_1[k] \end{bmatrix} \\
&= \begin{bmatrix} z[k-1] + \frac{T_s}{3600Q} I[k-1] \\ e^{-\frac{T_s}{R_1[k-1]C_1[k-1]}} i_{R1}[k-1] + (1 - e^{-\frac{T_s}{R_1[k-1]C_1[k-1]}}) I[k-1] \\ R_0[k-1] \\ R_1[k-1] \\ C_1[k-1] \end{bmatrix} + \begin{bmatrix} w_1[k-1] \\ w_2[k-1] \\ w_3[k-1] \\ w_4[k-1] \\ w_5[k-1] \end{bmatrix}
\end{aligned} \tag{5.13}
$$

$$
\begin{aligned}
y[k] &= V_t[k] \\
&= OCV(z[k-1]) + i_{R1}[k-1]R_1[k-1] + R_0[k-1]I[k-1] + v[k-1]
\end{aligned} \tag{5.14}
$$

where all the variables carry the same meaning as defined previously. As it can be seen from the terms like $e^{\frac{-T_s}{R_1[k-1]C_1[k-1]}} i_{R1}[k-1]$, the system was not linear. To build the Kalman filter steps similar to the ones described in Section 5.1 were followed. The values of $\hat{A}^-_{k-1}$ and $\hat{B}^-_{k-1}$ were altered to

$$
\hat{A}^-_{k-1} = \begin{bmatrix} 1 & 0 & 0 & 0 & 0 \\ 0 & e^{\frac{-T_s}{R_1[k-1]C_1[k-1]}} & 0 & \frac{T_s(i_{R1}[k-1]-I[k-1])e^{\frac{-T_s}{R_1[k-1]C_1[k-1]}}}{R_1[k-1]^2C_1[k-1]} & \frac{T_s(i_{R1}[k-1]-I[k-1])e^{\frac{-T_s}{R_1[k-1]C_1[k-1]}}}{R_1[k-1]C_1[k-1]^2} \\ 0 & 0 & 1 & 0 & 0 \\ 0 & 0 & 0 & 1 & 0 \\ 0 & 0 & 0 & 0 & 1 \end{bmatrix} \tag{5.15}
$$

$$
\hat{B}^-_{k-1} = \begin{bmatrix} 1 & 0 & 0 & 0 & 0 \\ 0 & 1 & 0 & 0 & 0 \\ 0 & 0 & 1 & 0 & 0 \\ 0 & 0 & 0 & 1 & 0 \\ 0 & 0 & 0 & 0 & 1 \end{bmatrix} \tag{5.16}
$$

where all variables hold the same meaning as previously defined. The values of $\hat{C}_k$ and $\hat{D}_k$ were found to be

$$\hat{C}_k = \begin{bmatrix} \left.\frac{\mathrm{d}OCV}{\mathrm{d}z}\right|_{z=z_k^-} & R_1 & I[k] & i_{R1}[k] & 0 \end{bmatrix} \tag{5.17}$$

$$\hat{D}_k = 1 \tag{5.18}$$

where all the variables have the definitions previously described.

5.2.2 JEKF for SOH Estimation

To include SoH estimation in the Joint Extended Kalman filter involved adding a state equation for the capacity of the cell. Similar to the circuit parameters, capacity, Q could be assumed to change slowly. This meant that the reciprocal 1/Q also changed slowly. Thus an additional state x_6 =1/Q was added to the state matrix and it had the system equation

$$x_6[k] = x_6[k-1] + w_6[k-1] \tag{5.19}$$

where the variables have the same meaning as described previously and the subscript accommodates the additional state. The values of $\hat{A}_{k-1}^-$ and $\hat{B}_{k-1}^-$ were altered slightly due to the addition of a new state x_6 to

$$\hat{A}_{k-1}^- = \begin{bmatrix} 1 & 0 & 0 & 0 & 0 & \frac{T_s I[k-1]}{3600} \\ 0 & e^{\frac{-T_s}{R_1[k-1]C_1[k-1]}} & 0 & \frac{T_s(i_{R1}[k-1]-I[k-1])e^{\frac{-T_s}{R_1[k-1]C_1[k-1]}}}{R_1[k-1]^2 C_1[k-1]} & \frac{T_s(i_{R1}[k-1]-I[k-1])e^{\frac{-T_s}{R_1[k-1]C_1[k-1]}}}{R_1[k-1]C_1[k-1]^2} & 0 \\ 0 & 0 & 1 & 0 & 0 & 0 \\ 0 & 0 & 0 & 1 & 0 & 0 \\ 0 & 0 & 0 & 0 & 1 & 0 \\ 0 & 0 & 0 & 0 & 0 & 1 \end{bmatrix} \tag{5.20}$$

$$\hat{B}_{k-1}^- = \begin{bmatrix} 1 & 0 & 0 & 0 & 0 & 0 \\ 0 & 1 & 0 & 0 & 0 & 0 \\ 0 & 0 & 1 & 0 & 0 & 0 \\ 0 & 0 & 0 & 1 & 0 & 0 \\ 0 & 0 & 0 & 0 & 1 & 0 \\ 0 & 0 & 0 & 0 & 0 & 1 \end{bmatrix} \tag{5.21}$$

where all variables hold the same meaning as previously defined. The values of $\hat{C}_k$ and $\hat{D}_k$ were found to be

$$\hat{C}_k = \left[\left. \frac{\mathrm{d}OCV}{\mathrm{d}z} \right|_{z=z_k^-} \quad R_1 \quad I[k] \quad i_{R1}[k] \quad 0 \quad 0 \right] \tag{5.22}$$

$$\hat{D}_k = 1 \tag{5.23}$$

where all the variables have the definitions previously described. The EKF steps described in Section 5.1 was applied to this joint system as well to estimate all the states.

Chapter 6

Results

This Chapter presents the Results and observations made in this thesis. The results are presented in a similar chronology to the chapters on the methodology followed. First, results from testing are presented, followed by the results from the modeling and the state estimation.

6.1 Testing

The testing data was studied to see if any trends were revealed for specific SOC windows. One of the quantities of interest was the capacity of the cell, this was both the charge and discharge capacity. Data on the capacity was collected before the tests were started, i.e. at the beginning-of-life (BOL) of the cell. The next RPT was conducted after 100 EFC and hence the next capacity data is after 100 EFC. After that since another 50 EFC were conducted the next capacity data was available at 150 EFC since the BOL.

6.1.1 Capacity

It was observed that the discharge capacity of the cells degraded the most for the (0-100) % SOC window. The next SOC window showing the most degradation in capacity was the window (25-100) %. The windows (50-100) % and (25-75) % showed a lower loss of capacity. Although the loss in capacity was comparable between the two windows, the (25-75) % SOC window was found to be slightly better when it comes to this aging metric after 150 cycles. The percentage loss in capacity after 100 EFC and then after 150 EFC is found in Table 6.1. The same data is presented visually in Figure 6.1 but converted into SoH. So the remaining capacity is indicated as a percentage of the initial capacity. It is to be noted that the capacity degradation is not linearly related to the number of cycles. The plot in Figure 6.1 is linear between 0-100 and 100-150 EFC only to have a plot to act as a visual aid for the data in Table 6.1.

Table 6.1: Discharge capacity degradation with cycling

Group	SOC Window	Cycles giving 100 EFC	Capacity decrease after 100 EFC [%]	Capacity decrease after next 50 EFC [%]
Group 1	(0-100) %	100	4.8	2.3
Group 2	(25-100) %	133.3	4	1
Group 3	(50-100) %	200	2.3	1.35
Group 4	(25-75) %	200	2.5	1

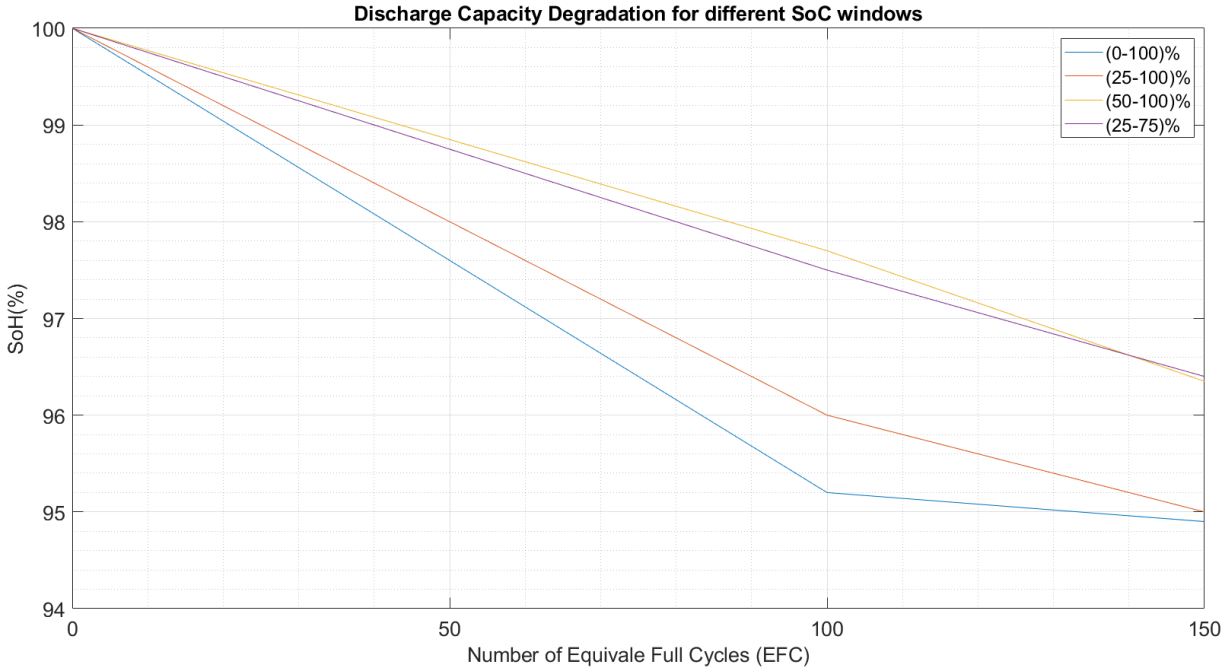

Figure 6.1: Discharge capacity degradation for different SOC windows

It was observed that the charge capacity of the cells degraded the most for the (0-100) % SOC window. The next SOC window showing the most degradation in capacity was the window (25-100) %. The windows (50-100) % and (25-75) % show lesser loss of capacity. Although the loss in capacity was comparable between the two windows, the (50-100) % SOC window was found to be slightly better when it comes to this aging metric after 150 cycles. The percentage loss in capacity after 100 EFC and then after 150 EFC is found in Table 6.2. The same data is presented visually in Figure 6.2 but converted into SoH. So the remaining charge capacity is indicated as a percentage of the initial capacity. It is to be noted that the capacity degradation is not linearly related to the number of cycles. The plot in Figure 6.2 is linear between 0-100 and 100-150 EFC only to have a plot to act as a visual aid for the data in Table 6.2.

Table 6.2: Charge capacity degradation with cycling

Group	SOC Window	Cycles giving 100 EFC	Capacity decrease after 100 EFC [%]	Capacity decrease after next 50 EFC [%]
Group 1	(0-100) %	100	5.6	2.5
Group 2	(25-100) %	133.3	4.8	3.4
Group 3	(50-100) %	200	3.1	1.4
Group 4	(25-75) %	200	3.6	1

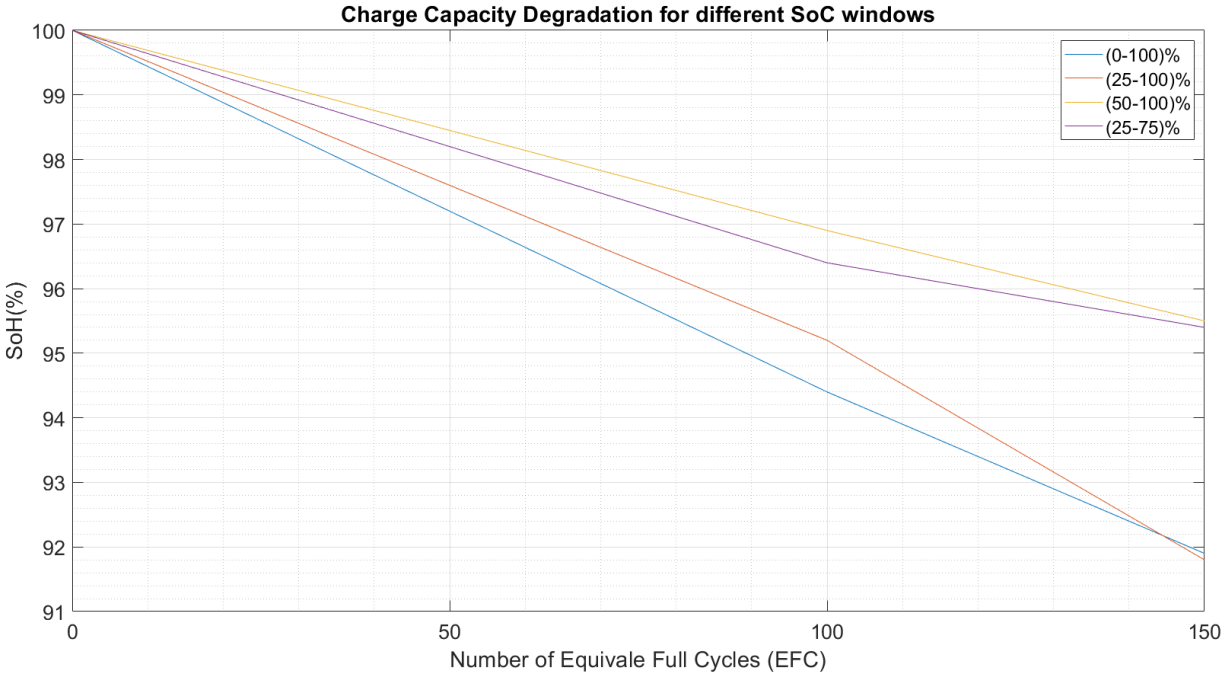

Figure 6.2: Charge capacity degradation for different SOC windows

An observation to be made was that when the cell was cycled at a much lower SOC the capacity degradation was higher. Thus, discharging a cell to SOC in the area of 25 % and lower makes the cell age faster. Thus it may be better to cycle the cell between higher SOC values such as (50-100) % to improve the lifetime of the cell. In [19] it is established that with the increase in depth of discharge (DoD) the capacity degradation increases. This could be one way of explaining the higher capacity degradation at lower SoC. In [20] the main mechanism causing this is said to be the expansion and contraction of the electrodes leading to the cracking of the Solid electrolyte interface (SEI) which causes more rapid capacity degradation. The larger the SoC swing window, the larger the stresses experienced by the SEI layer, and this leads to more fracturing of the SEI layer. This could also explain why the smaller SoC windows in Groups 3, and 4 with 50% SoC swings experienced lower capacity degradation than SoC windows in Groups 1 and 2 with 100% and 75% SoC swings.

Another observation to be made was that the charge capacity degrades faster than the discharge capacity and this leads to an increase in the coulombic efficiency of the

cell as the cell ages. On average the coulombic efficiency goes from being 0.98 in the BOL to being 0.991 after 100 EFC to being around 0.994 after 150 EFC. This can be explained by that the initial cycling of the cell leads to the formation of the SEI layer on the anode which reduces the energy lost to side reactions between the electrode and electrolyte thus improving the efficiency of the cell. In [21] it is noted that a slight increase in coulombic efficiency is observed during the initial cycling of Li-ion batteries.

6.2 Modelling

6.2.1 SOC-OCV Curve

In the original charge SOC-OCV curve the charge OCV (solid blue) is higher than the discharge OCV (solid green) as seen in Figure 6.3. This is as expected from the phenomenon of hysteresis, i.e. at the same SOC, a different OCV can result based on the history of the cell. Then the charge OCV curve obtained through measurement includes the small voltage drop that exists even when the small current is used. Thus the IR compensated Charge OCV (dotted blue) is lower than what is measured. Both cover the lower range of SOC but do not go all the way to 100 % SOC as seen in Figure 6.3.

The discharge OCV curve (green) obtained through measurement includes the small voltage drop that exists even when a small current is used. Thus the IR compensated discharge OCV (dotted green) is higher than what is measured. Both cover the higher range of SOC but do not go all the way to 0 % SOC as seen in Figure 6.3.

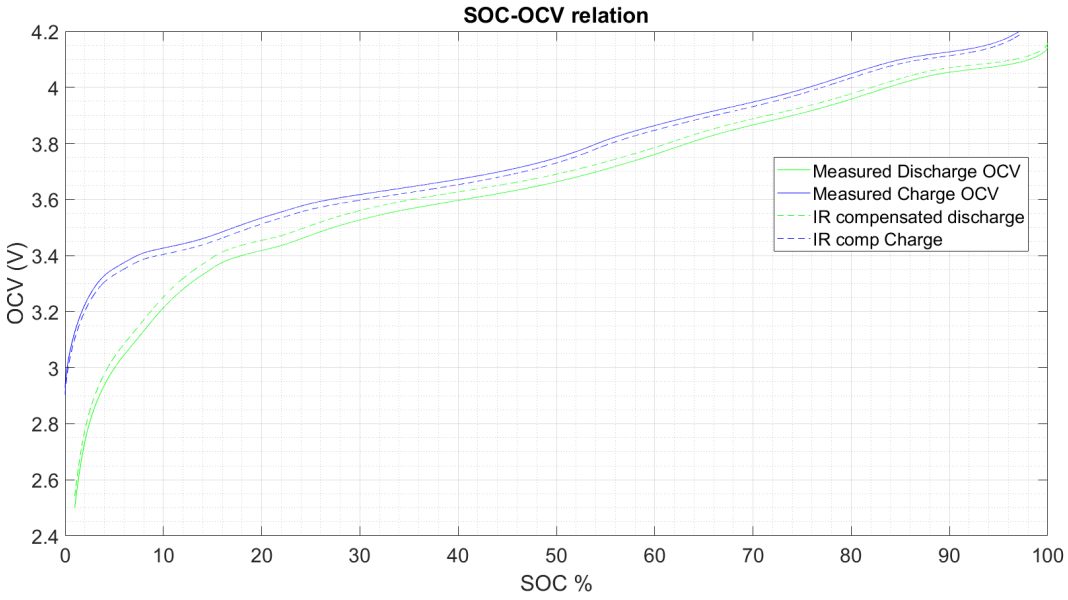

Figure 6.3: IR drop compensated OCV

The blended OCV-SOC curve (red) is presented in Figure 6.4. It is seen that in the 0-50 % range of SOC, it is more aligned with the charge OCV and in the 50-100 % range it is more aligned with the discharge OCV. This is expected from the way that

the blended OCV-SOC curve is calculated.

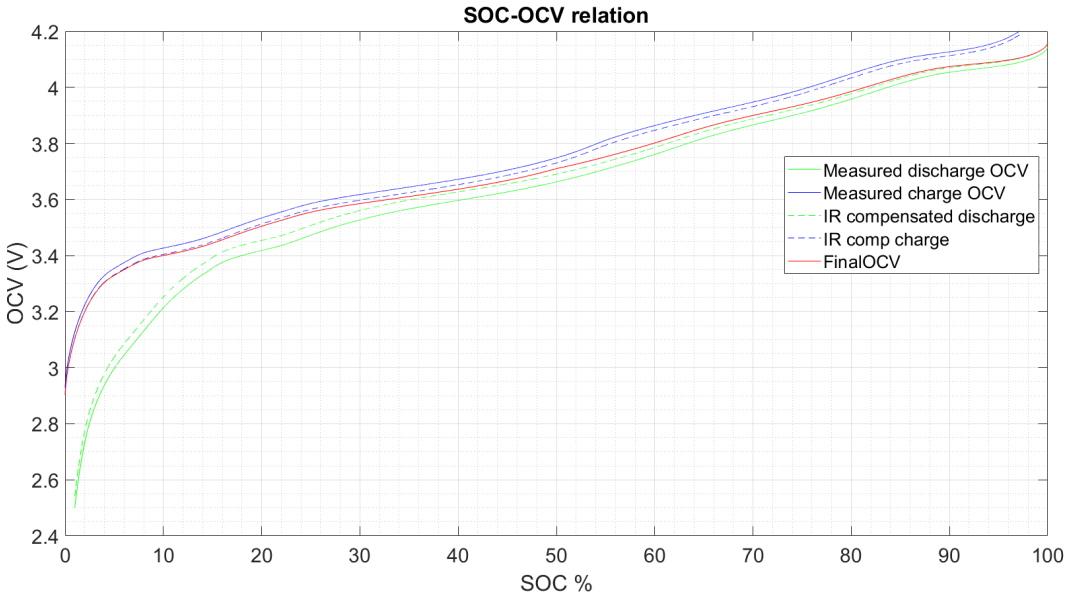

Figure 6.4: Final averaged OCV

6.2.2 Model Parameters

The model parameters obtained are plotted against the SOC levels in Figure 6.5 and 6.6 for the 1 RC model. In Figure 6.5, the parameters obtained from the physical calculation are presented while in Figure 6.6 the results from the Matlab Optimizer are presented. It is also observed that the value of R_1 is highest at the lower and higher SOCs. A possible explanation could be that at low SoC there are fewer Li-ions available and this increases the resistance. At higher SoC there is more energy available for side reactions, these side reactions can increase the resistance of the cell. In [22] it was found that the internal resistance of the cell is higher at very low and very high SoCs. It is also observed that the physically calculated parameters change more steadily than the parameters obtained from the optimizer. This is understandable since the physical calculation takes into consideration what the parameters affect individually while the Matlab Optimizer is a mathematical solver and finds the best solution of a combination of parameters that gives the measured output.

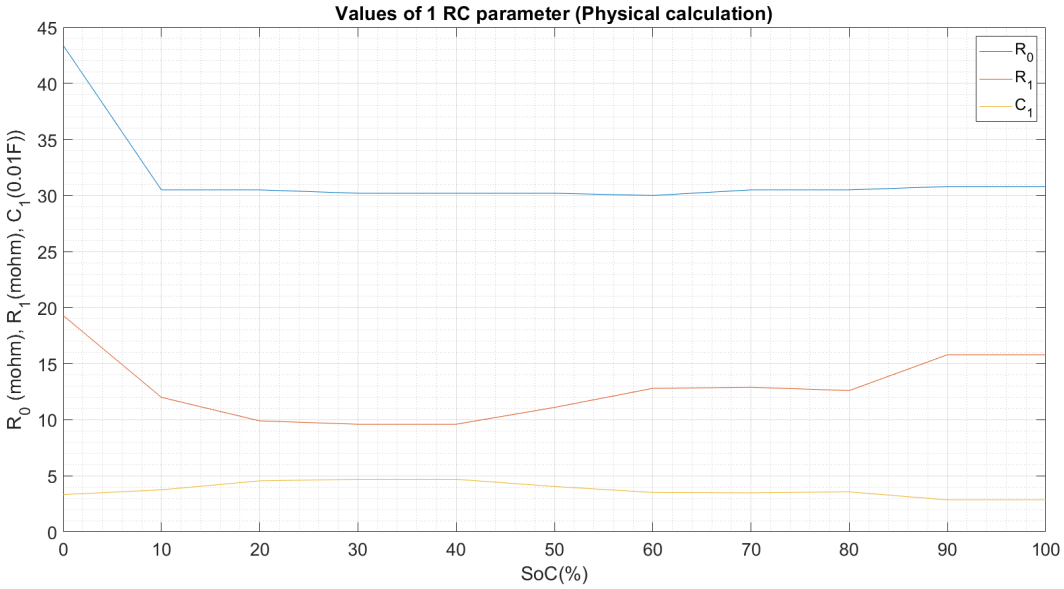

Figure 6.5: 1 RC parameter values calculated physically

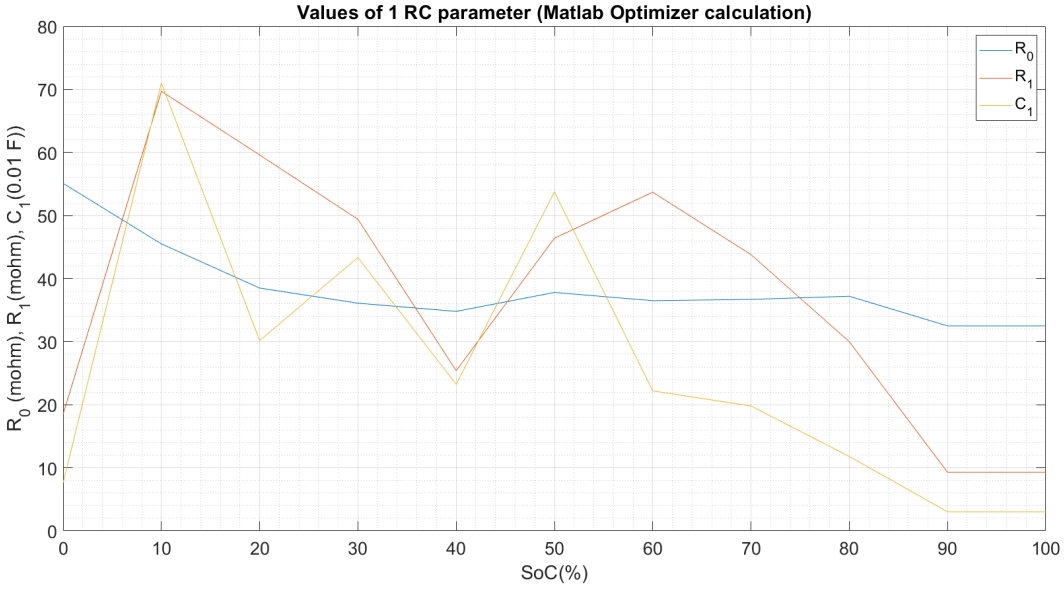

Figure 6.6: 1 RC parameter values calculated through MATLAB optimizer

In Figure 6.7, the results obtained from the MATLAB optimizer for the 2RC model parameters are presented. It is seen that the value of R_0 is higher at lower and higher SOCs as previously described.

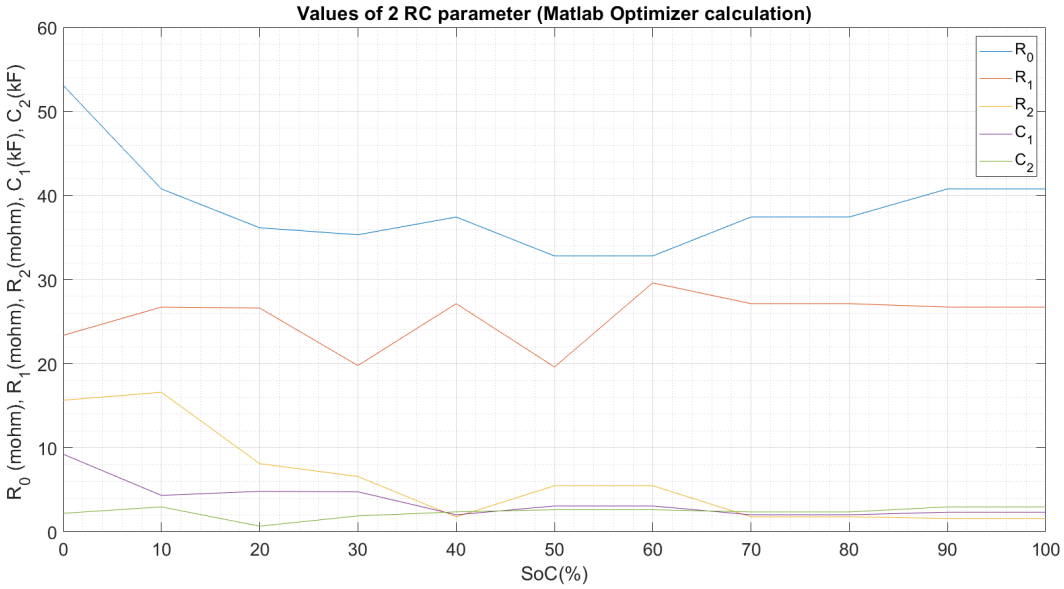

Figure 6.7: 2 RC parameter values calculated through MATLAB optimizer

6.2.3 1 and 2 RC Model

In Figure 6.8 the results are presented when the 1RC and 2RC models are simulated with HPPC current as input (window 1). The output from both 1 RC and 2 RC is shown along with the actual measured output voltage. It is observed that both 1 RC and 2 RC models follow the actual output closely. From the SOC-OCV curves in Section 6.2.1 and Model Parameters presented in 6.2.2 the methods used in the results presented henceforth vary the SOC-OCV curve based on whether the cell is charged or discharged and the manually calculated model parameters for a 1RC model. It was found by trying different settings that this combination worked well, the differences between other set-ups were not significant and are not presented in this report.

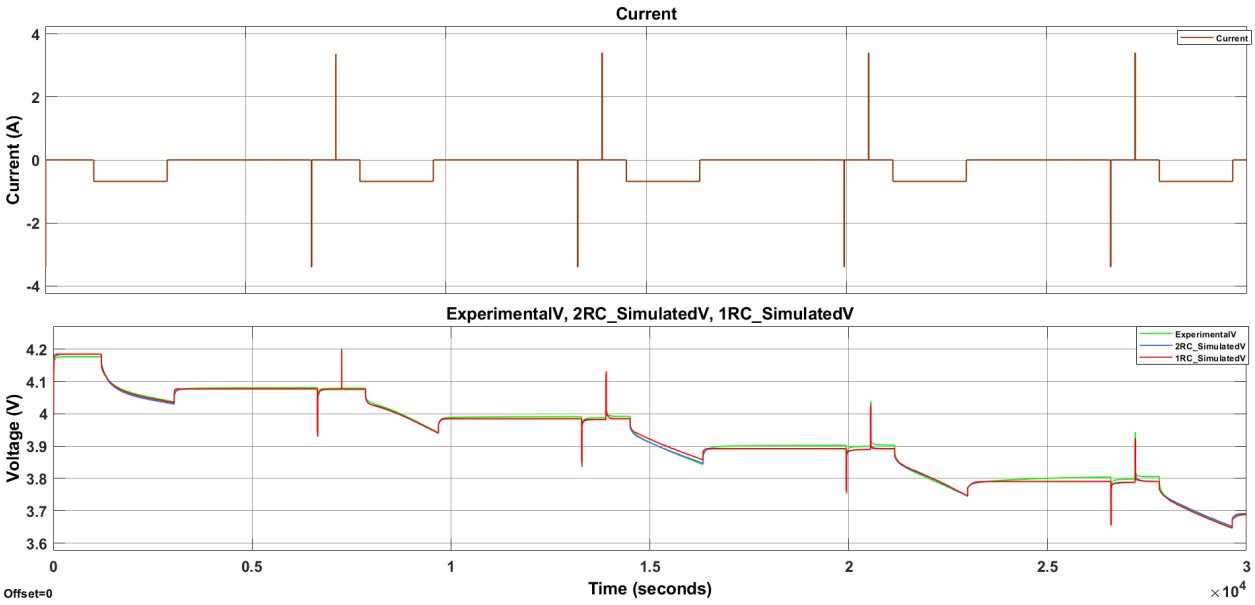

Figure 6.8: 1RC model and 2 RC model terminal voltage compared to the measured terminal voltage for HPPC data

Since the parameters of the models were chosen with the HPPC test as a base, it is insufficient to validate the models on the same data. The additional WLTP cycle current that the models were validated against is shown in Figure 6.9. The data used is for 1 WLTP cycle. The 1 RC and 2 RC simulated output voltages are compared against the actual measured voltages in Figure 6.9 in the second window.

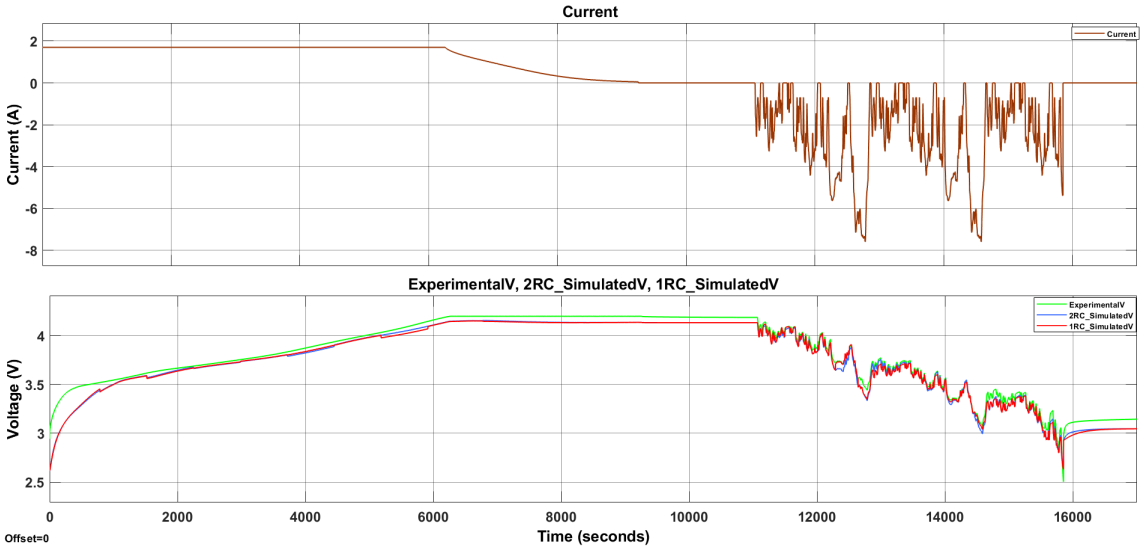

Figure 6.9: 1RC model and 2 RC model terminal voltage compared to the measured terminal voltage for WLTP data

Figure 6.10 highlights a zoomed-in section of the HPPC pulse to show the difference observed in the 1 RC and 2 RC models in capturing the slow changes in the output voltage. It can be seen that the 2 RC circuit does a better job of capturing these changes than the 1 RC model.

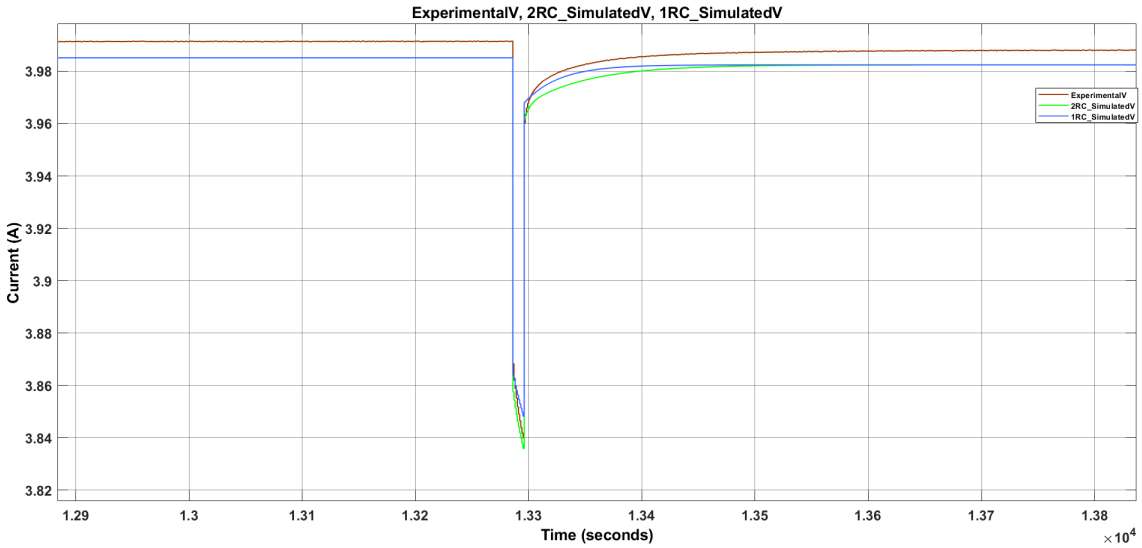

Figure 6.10: 1RC model and 2 RC model comparison in capturing the characteristics

Table 6.3 summarizes the results of the 1 RC and 2 RC models using root mean square error (RMSE). It was seen that the 1 RC circuit is slightly more accurate than the 2 RC model for the HPPC data. However, the 2 RC model was more accurate than the 1 RC model for the WLTP data. It was seen that when the lower SOC levels (0 %-20 %) are excluded in the HPPC data the accuracy of the models improves a lot. Thus the models were more accurate in the higher SOC levels. In general, the difference in accuracy between the 1 RC and 2 RC models was low and the 1 RC circuit worked well enough and compensated for the errors by being a computationally light model. Thus this was the model that was explored further for the state estimations.

Table 6.3: RMSE error compared for 1RC and 2RC

Test	HPPC (0-100) % SOC	HPPC (20-100) %	WLTP
Model	**RMSE (in V)**		
1 RC model	0.009	0.0068	0.048
2 RC model	0.0103	0.007	0.039

6.3 SOC Estimation

For the SOC Estimation from the Extended Kalman Filter, the value the SOC is compared to is the one obtained from Coulomb counting. The Kalman filter is a trade-off between relying on the system equations or model and relying on the measurements from the test data. The results in this section, highlight how the tuning of the Kalman filter gave different results - some more true to the system model and some more true to the test data.

6.3.1 SOC Estimation with Fixed Parameters

Results were obtained for different tunings of the Kalman filter. The choice of the values of Σ_V and Σ_W affects the Kalman filter and its results. Since Σ_W represents how reliable the system equation (coulomb counting is), a large Σ_W relative to Σ_V gave larger fluctuations and deviation from the Coulomb counting. However, the difference in the estimation of terminal voltage, $\hat{y}$, and the measured V_t from the test was small. Conversely, a small Σ_W relative to Σ_V gave a SOC estimation closer to that of the coulomb counting. $\hat{y}$ deviates more from V_t in this case.

Table 6.4 shows the two different cases whose results are shown here. It shows the values of Σ_W and Σ_V and the errors in the SOC estimation and estimated output for each case. In Figures 6.11 to 6.14 the figures are presented concerning this table.

Table 6.4: Comparing two tunings of the Kalman filter

Case	Σ_W	Σ_V	RMSE in $\hat{z}_k^+$ (p.u.)	RMSE in $\hat{y}$ (V)
Case 1	[1x10^{-9}, 0; 0, 10]	0.01	0.0138	0.0146
Case 2	[1x10^{-7}, 0, 0, 10]	1x10^{-9}	0.0320	0.0077

Figure 6.11 depicts the SOC estimation from the EKF w.r.t. to the SOC calculated through coulomb counting for Case 1. Figure 6.12 shows the estimation of terminal voltage in the EKF in Case 1 w.r.t. the actual measurement of cell terminal voltage. Figure 6.13 depicts the SOC estimation from the EKF w.r.t. to the SOC calculated through coulomb counting for Case 2. Figure 6.14 shows the estimation of terminal voltage in the EKF in Case 1 w.r.t. the actual measurement of cell terminal voltage.

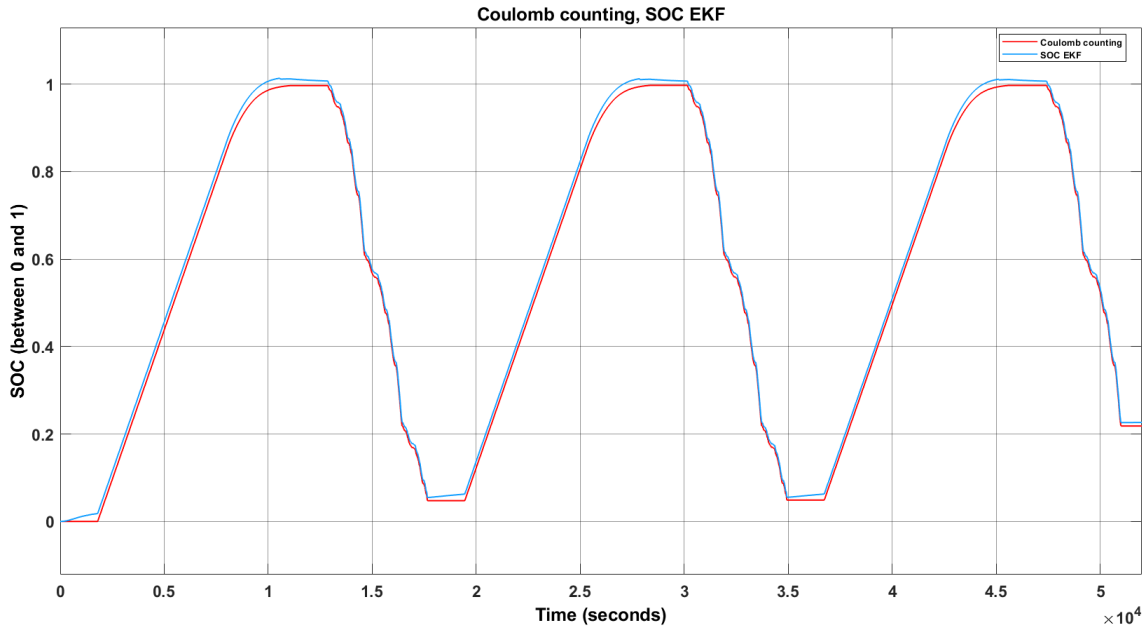

Figure 6.11: SOC estimation from EKF for case 1

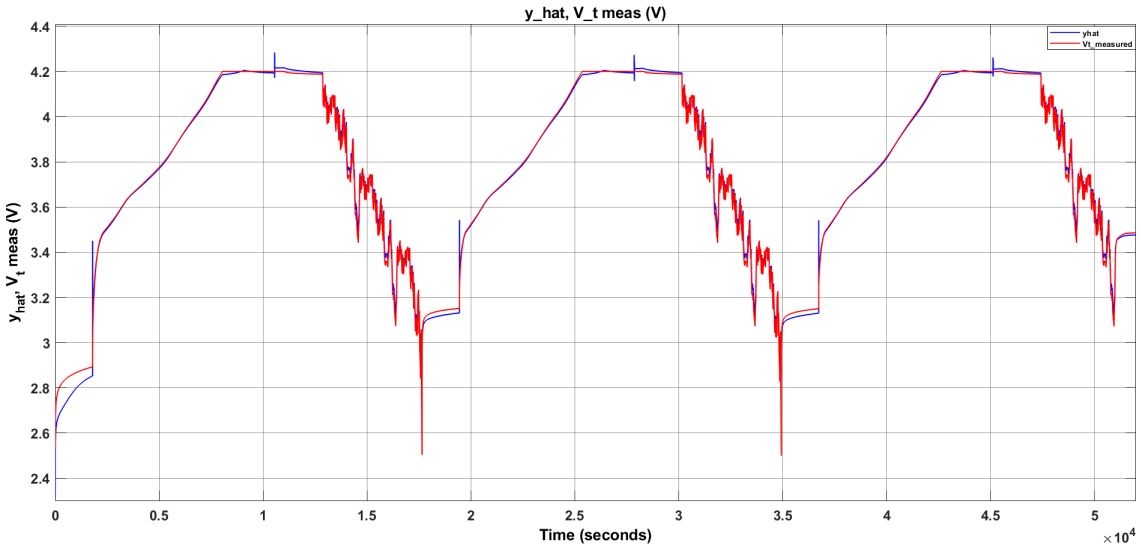

Figure 6.12: V_t v/s $\hat{y}$ from EKF for case 1

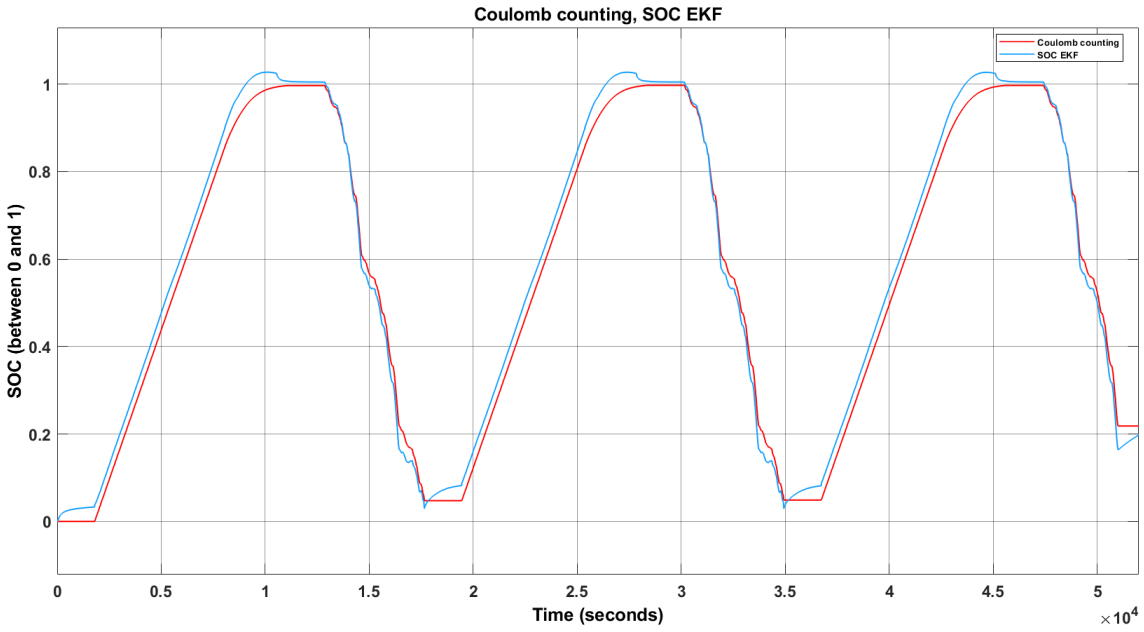

Figure 6.13: SOC estimation from EKF for case 2

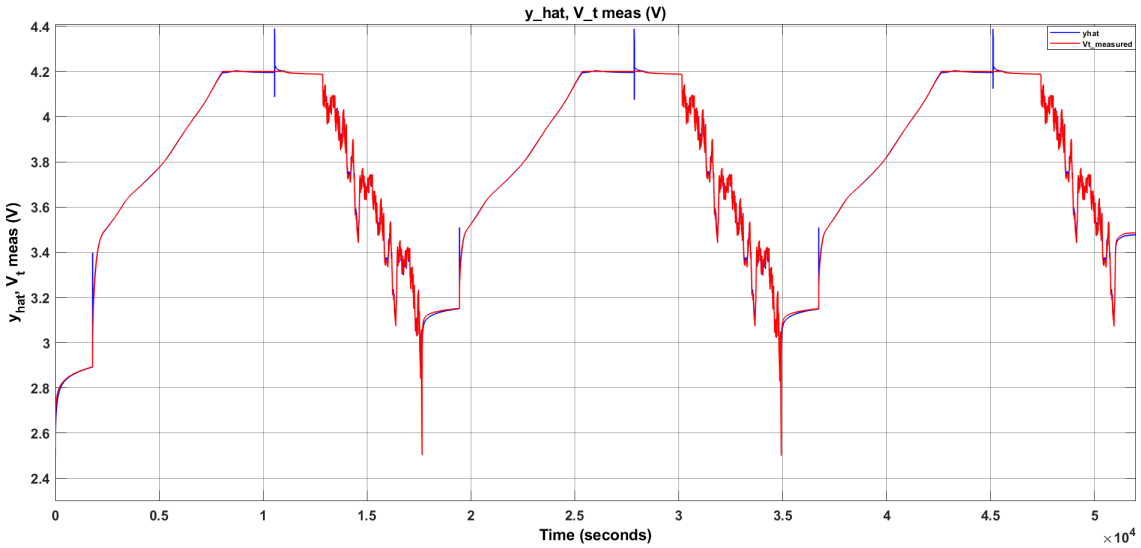

Figure 6.14: V_t v/s $\hat{y}$ from EKF for case 2

Figure 6.15 depicts the SOC (z state) estimation from the EKF. In this case, the SOC of the cell was initialized to an incorrect value. However, using the measurement of the terminal voltage and comparing it to the y estimated within the Kalman filter, the EKF can converge to the actual value of SOC (obtained from coulomb counting) quite soon and then it follows this SOC. However, it is visible that there is an offset in the estimated SOC and actual SOC. The reason behind this could be the large error in the initial estimate. The Kalman filter tries to compensate for this error but might not be entirely succeeding. One of the reasons might be that the system model does not describe the cell behavior completely accurately. Another reason could be that the convergence to the actual SOC will take more time than shown in the figure since the KF does not converge instantaneously.

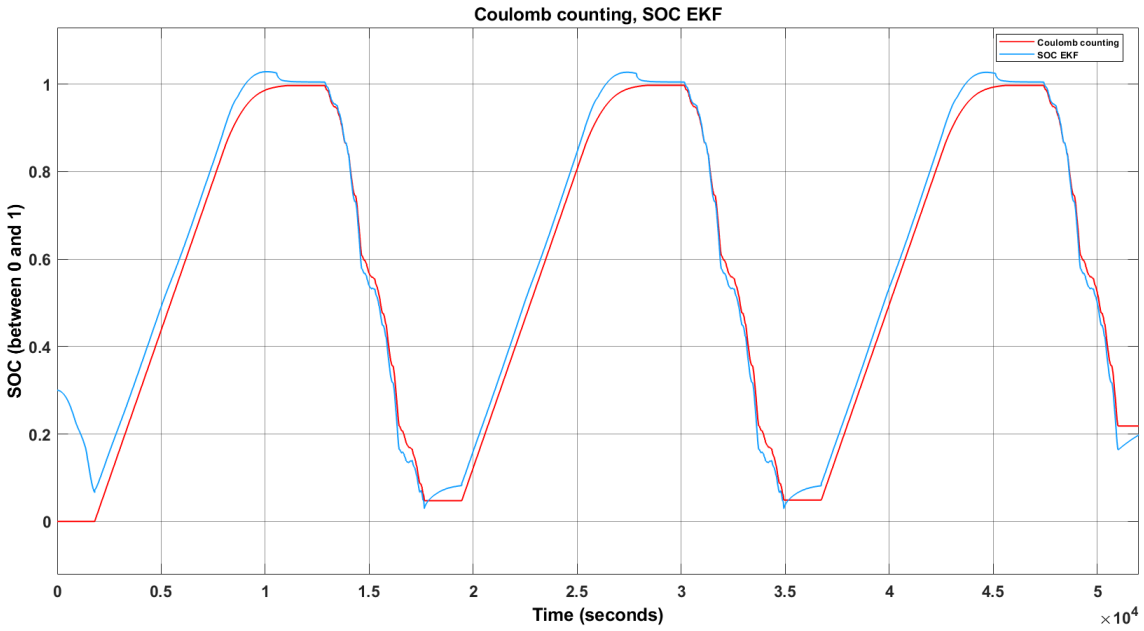

Figure 6.15: SOC estimation from EKF when initialized far from real value

6.3.2 Estimation with Joint EKF

With the addition of more states to the EKF to make the joint extended Kalman filter, it grew trickier to tune the Kalman filter. Figures 6.16 to 6.17 depict the SOC, R_0, and capacity Q estimated by the joint Kalman filter. In this case the values of Σ_V was [1] and of Σ_W was $\begin{bmatrix} 1\text{x}10^{-4} & 0 & 0 & 0 \\ 0 & 1 & 0 & 0 \\ 0 & 0 & 1\text{x}10^{-4} & 0 \\ 0 & 0 & 0 & 1\text{x}10^{-9} \end{bmatrix}$. Figure 6.16 shows the estimation of SOC for this scenario. The RMSE in $\hat{z_k}^+$ was 0.0371 p.u. and the RMSE in $\hat{y}$ was 0.0092 V in this case. This is similar to the errors in the EKF in Case 2 in Section 6.3.1. Thus the current tuning of the JEKF did not give significant improvement over the EKF. Figure 6.17 shows the variations in SOH which are quite low as expected. Figure 6.18 shows the estimation of R_0 by the JEKF. The value calculated is mathematical and hence negative sometimes, this does not hold physical meaning.

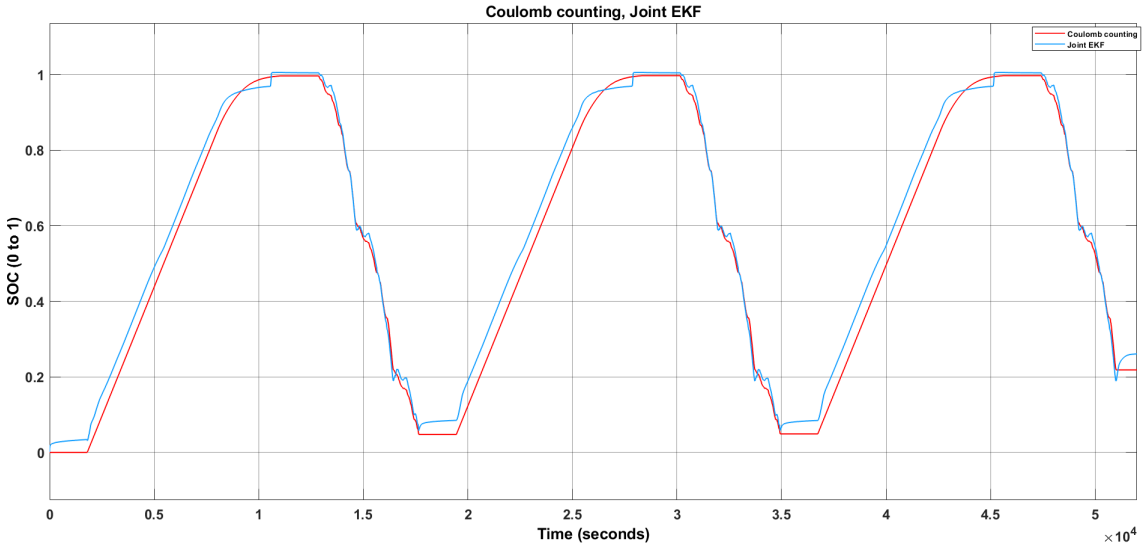

Figure 6.16: SOC estimation from the JEKF

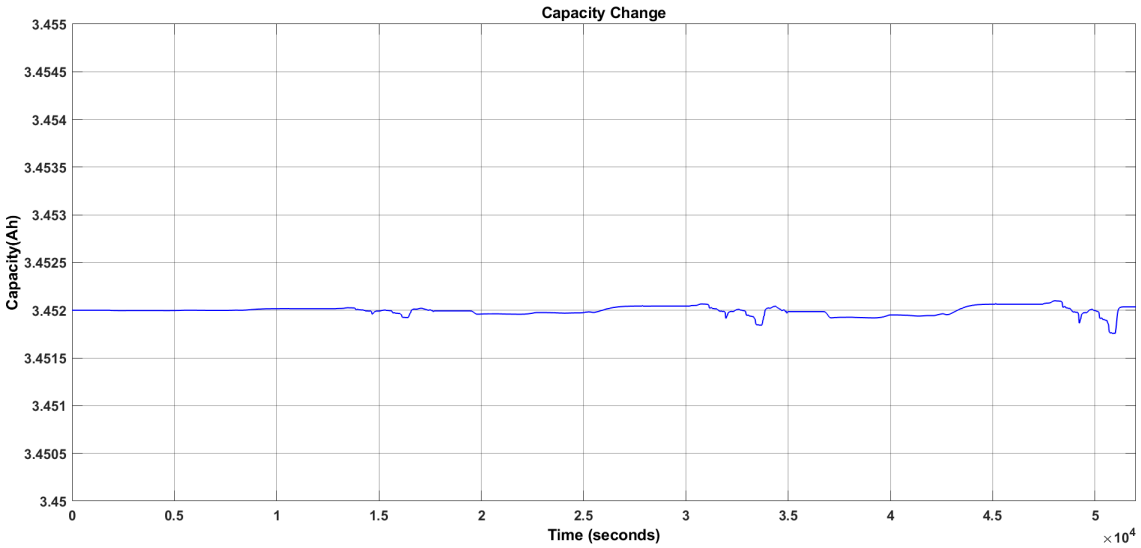

Figure 6.17: Capacity estimation from the JEKF

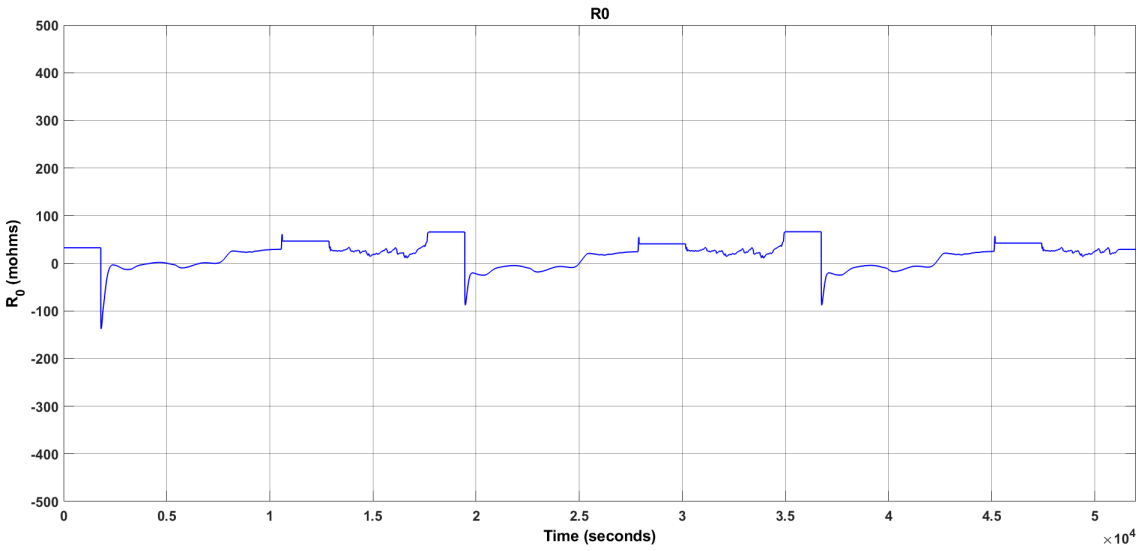

Figure 6.18: Estimation of R_0 from the JEKF

Chapter 7

Conclusion

This master thesis work constituted of different elements around Li-ion cell technology. It began with a Literature review and planning phase to understand the basics and topics around Li-ion cells, testing, modeling, and Kalman filters. A time plan was developed based on the predicted tasks.

The setting up for testing and collecting data on Li-ion cells chosen for the thesis followed. Cell testing was done by preparing the test harness and developing a test methodology to include Reference Performance Tests and Dynamic Cycling with WLTP to get the best data. The script to perform the tests was also written.

The test data obtained was then processed and used to derive the SOC-OCV curve and different methods attempted to obtain the model parameters for electric equivalent circuits of the cell in the beginning-of-life of the cell. 1 RC and 2 RC electric models were compared for accuracy and complexity. It was decided to continue with the 1 RC model.

State of Charge estimation was implemented using an Extended Kalman Filter. The effect of tuning on the results of the Kalman filter was observed. An inclusion of capacity and model parameter estimation was done and a Joint extended Kalman filter was designed and tuned. The theory, methodology, and results obtained were documented in a report format. Considering room for improvement and challenges, a Chapter 8 on Future work is included in the report. The ethical and environmental aspects of the thesis are also reflected upon in Chapter 9.

Chapter 8

Future work

During the thesis, some challenges and areas with more room for improvement were identified. These are detailed below.

- One aspect to be further investigated is the inclusion of regenerative braking in the WLTP tests conducted. This, in combination with the data already collected, will provide the foundation for investigating the impact of regenerative braking on the general lifetime of lithium-ion battery cells.
- The Joint Extended Kalman Filter includes both values that change rapidly and ones that change slowly. The Joint Extended Kalman filter becomes complex to both tune and implement. Instead, Dual Kalman filters can be designed. One for the fast-changing parameters and one for the slow changing which is updated at a lower frequency. There has to be an information exchange between the two Kalman filters.
- Since to have physical meaning resistance and capacity must be positive, with time capacity can only decrease and SOC must be limited to between 0-1, constraints must be added on the states in the state estimation.
- Temperature is not considered in this thesis. It plays a significant role in the behavior of Li-ion cells and its influence can also be modeled.
- Apart from the Extended Kalman filter there are other filters such as the Unscented Kalman filter and the Particle filter which show promise as being an improvement over the EKF and can also be tried to solve the same problem.

Chapter 9

Discussion

9.1 Environmental Aspects

For the world to move towards a more sustainable future, significantly reducing global CO_2 emissions will be needed. The subject of this thesis concerns energy storage using batteries with a main focus on the automotive industry. The subject of significantly reducing the emissions from the automotive and transport sector is one of the main areas of focus within the industry, academia, and politics. Over the past decade, alternatives to conventional combustion engines have been explored and the market is now rapidly moving towards battery electric vehicles (BEV). BEVs are often referred to as having zero emissions but that is only true when the car is driving. However, that is not true during the full life cycle of the BEV where the source of the electricity, raw materials, production process, logistics, and end-of-life recycling and scrapping are very important to consider when determining the total CO_2 emissions of the BEV during its lifetime. This means that efficient use of materials and energy for BEVs is very important to reduce the global CO_2 emissions.

The first aspect mentioned above concerns efficient material use where materials that have significant CO_2 emissions during their sourcing and production must be used efficiently. Efficient use means both limiting the amount of material used but also limiting the number of times the specific component will have to be replaced during the lifetime of the vehicle. When it comes to battery cells, several raw materials have to be mined, transported, and manufactured into a cell. This means that using every cell to the maximum of its potential whilst simultaneously ensuring that the lifetime is maximized is very important. This means reducing the amount of cells needed throughout the lifetime of the BEV reducing the amount of material with high CO_2 emissions and reducing the number of times the battery has to be replaced. It is however not only the battery cells themselves where more efficient utilization of materials will reduce CO_2 emissions, also having a less complex BMS will reduce the computational power needed. This will lead to less electronics needed in the system and also less energy use from these systems.

The second aspect is the CO_2 emissions caused by the production of the electricity

needed to charge the batteries. While the battery system designer cannot control the source of the electricity used, ensuring that the charging and discharging of the battery are efficiently done, minimizing the losses and therefore reducing the amount of electricity used during the lifetime of the battery system. In that way, electric vehicles operating in regions where the electricity production is CO_2 emission heavy will minimize their carbon footprint caused by the electricity production.

There is also another aspect which is safety in BEVs where the role of the BMS is to keep the battery operating within a window that is considered safe. To reduce the safety margins needed in the BMS, having accurate information about the state of the cells is crucial and therefore being able to estimate the cell parameters throughout the lifetime of the cell is crucial. In addition, better knowledge of the battery cells will help with both diagnostics and extending the lifetime of the battery by operating it within a range that limits the degradation of the cells.

9.2 Ethical Aspects

Apart from the environmental issues, there are also ethical issues that must be considered. The raw materials used when producing battery cells such as Cobalt, Nickel, and Lithium are mined in areas where human rights and fair working conditions may be a concern. Also, there are concerns regarding the environmental impact of mining the material on a local level. Sustainable mining and production is generally a costly procedure and therefore it will not be as profitable as other options for companies. This is another reason for the designers to completely avoid or at the very least ensure that the use of these materials is kept to a minimum.

Bibliography

[1] R. Jung, M. Metzger, F. Maglia, C. Stinner, and H. A. Gasteiger, "Chemical versus electrochemical electrolyte oxidation on nmc111, nmc622, nmc811, lnmo, and conductive carbon," *The journal of physical chemistry letters*, vol. 8, no. 19, pp. 4820–4825, 2017.

[2] Y. Wang, J. Tian, Z. Sun, *et al.*, "A comprehensive review of battery modeling and state estimation approaches for advanced battery management systems," *Renewable and Sustainable Energy Reviews*, vol. 131, p. 110 015, 2020.

[3] X. Hu, S. Li, and H. Peng, "A comparative study of equivalent circuit models for li-ion batteries," *Journal of Power Sources*, vol. 198, pp. 359–367, 2012.

[4] T. Feng, L. Yang, X. Zhao, H. Zhang, and J. Qiang, "Online identification of lithium-ion battery parameters based on an improved equivalent-circuit model and its implementation on battery state-of-power prediction," *Journal of Power Sources*, vol. 281, pp. 192–203, 2015.

[5] G. L. Plett, "Extended kalman filtering for battery management systems of lipb-based hev battery packs. part 2. modeling and identification," *Journal of Power sources*, vol. 134, no. 2, pp. 262–276, 2004.

[6] ——, "Extended kalman filtering for battery management systems of lipb-based hev battery packs: Part 1. background," *Journal of Power sources*, vol. 134, no. 2, pp. 252–261, 2004.

[7] M. U. Cuma and T. Koroglu, "A comprehensive review on estimation strategies used in hybrid and battery electric vehicles," *Renewable and Sustainable Energy Reviews*, vol. 42, pp. 517–531, 2015.

[8] G. L. Plett, "Extended kalman filtering for battery management systems of lipb-based hev battery packs: Part 3. state and parameter estimation," *Journal of Power sources*, vol. 134, no. 2, pp. 277–292, 2004.

[9] RISE, *Physics-based modelling of batteries*, `https://www.ri.se/en/what-we-do/services/physics-based-modelling-of-batteries`.

[10] J. Forman, S. Bashash, J. Stein, and H. Fathy, "Reduction of an electrochemistry-based li-ion battery model via quasi-linearization and padé approximation," *Journal of The Electrochemical Society*, vol. 158, A93–A101, Feb. 2011. DOI: `10.1149/1.3519059`.

[11] M. Guo, G. Sikha, and R. White, "Single-particle model for a lithium-ion cell: Thermal behavior (vol 158, pg a122, 2011)," *Journal of The Electrochemical Society*, vol. 158, Jan. 2011. DOI: `10.1149/1.3521314`.

[12] G. L. Plett, *Equivalent Circuit Cell Models*, http://mocha-java.uccs.edu/ECE5710/ECE5710-Notes02.pdf, Jun. 2011-2018.

[13] S. Tamilselvi, G. Selvaraj, K. Natarajan, *et al.*, "A review on battery modelling techniques," *Sustainability*, vol. 13, p. 10 042, Sep. 2021. DOI: 10.3390/su131810042.

[14] G. L. Plett, *Introduction to Kalman Filters*, http://mocha-java.uccs.edu/ECE5550/ECE5550-Notes01.pdf, 2009-2018.

[15] ——, *NonLinear Kalman Filters*, http://mocha-java.uccs.edu/ECE5550/ECE5550-Notes06.pdf, 2009-2018.

[16] LG Chem, *Product Specification INR18650MJ1*, https://power.tenergy.com/content/datasheet/30708_datasheet.pdf, Jun. 2016.

[17] G. T. Akinyokun, *Adaptive Modelling and State Estimation Algorithm for Lithium-Ion Battery Management in Sustainable Energy Applications*, Aug. 2022.

[18] G. L. Plett, *Dual and Joint EKF for Simultaneous SOC and SOH Estimation*, http://mocha-java.uccs.edu/dossier/RESEARCH/2005evs21b-.pdf.

[19] R. D. Deshpande and K. Uddin, *Physics inspired model for estimating 'cycles to failure'as a function of depth of discharge for lithium ion batteries*, 2021.

[20] Deshpande, Rutooj D and Bernardi, Dawn M, *Modeling solid-electrolyte interphase (SEI) fracture: coupled mechanical/chemical degradation of the lithium ion battery*, 2017.

[21] J. Xiao, Q. Li, Bi, *et al.*, "Understanding and applying coulombic efficiency in lithium metal batteries," *Nature energy*, 2020.

[22] Kim, Daehyun and Koo and others, *Second-order discrete-time sliding mode observer for state of charge determination based on a dynamic resistance li-ion battery model*, 2013.